QATAR UNIVERSITY

COLLEGE OF ARTS AND SCIENCES

THE EFFECT OF NIOBIUM ON THE PHASE STABILITY AND MECHANICAL PROPERTIES OF NICKEL-BASED HIGH ENTROPY ALLOYS

BY

FATMA AL MAADEED

A Thesis Submitted to

the College of Arts and Sciences

in Partial Fulfillment of the Requirements for the Degree of

Masters of Science in Material Science and Technology

January 2023

COMMITTEE PAGE

The members of the Committee approve the Thesis of

Fatma Al Maadeed defended on 15/01/2022.

_____

Dr. Khaled Youssef
Thesis/Dissertation Supervisor

_____

Dr. Aboubakr M. Abdullah Ali
Committee Member

_____

Dr. Mohamed Korany Ibrahim Hassan
Committee Member

Approved:

_____

Ahmed Elzatahry, Dean, College of Arts and Sciences

ABSTRACT

AL MAADEED, FATMA, M., Masters : June : 2022, Material Science and Technology Title: THE EFFECT OF NIOBIUM ON THE PHASE STABILITY AND MECHANICAL PROPERTIES OF NICKEL-BASED HIGH ENTROPY ALLOYS

Supervisor of Thesis: Dr. Khaled Youssef.

A fundamental understanding of the mechanisms of phase stability of high entropy alloys (HEAs) and the influence of refractory elements is a recent topic of active research. This study investigates the effect of Niobium (Nb), as a refractory element, on the phase stability and mechanical properties of NiCoCrAlNb HEAs. In this thesis, $Ni_{0.55}CoCrAlNb_x$ (x= 0, 0.01, 0.03, 0.05) high entropy alloys are prepared by using a vacuum arc melting technique. X-ray diffraction results demonstrate a single solid solution phase FCC in all samples. The addition of Nb content is studied through thermomechanical assessments and microstructure processing. Remarkable tensile properties were achieved for the HEA with 5% Nb content. The thermomechanical treatments were optimized, and the best combination of mechanical properties was obtained at an aging temperature of 950°C for one hour. Significant improvements are detected in tensile properties as the Nb content is increased. The yield and ultimate strength values of the optimized sample were found to be 1050 MPa and 1534 MPa, respectively. All the specimens aged at 950°C had a good tensile ductility of 34%. This thesis indicates that the properties of HEAs could be well tailored using thermomechanical and microstructure management for a high-performance HEA in industrial engineering applications.

DEDICATION

To my father, for his belief in me and the high hopes he has for the future. To my mother, for her support and ongoing encouragement to help me complete my degree. To my siblings and friends: thank you for the support, laughter, and sincere conversations. To my travel buddy, Dina, who has the sweetest soul, I dedicate this section. Thank you for making this experience unique, bearable, and lovely.

ACKNOWLEDGMENTS

I would like to express my deepest appreciation and gratitude to my thesis supervisor, Dr. Khaled Youssef, for providing me with the opportunity to conduct my thesis under his guidance and for his continuous academic support and mentorship. His invaluable insights and expertise have greatly contributed to the success of this research.

I would also like to extend my sincere thanks to Ms. Farah Elmakaty, for her assistance and support in the laboratory. Her knowledge and expertise have been of great help throughout the experimental work.

I am also grateful to my thesis committee members for their constructive comments and suggestions, which have helped to improve the quality of this thesis.

Special thanks are also due to the Central Laboratory Unit and Center for Advanced Materials at Qatar University for their assistance with the experimental work. Specifically, I would like to express my appreciation to Ms. Rokaya Abdeltty for her support and guidance throughout the process.

I would also like to express my gratitude to the external examiner for his insightful and helpful comments on the thesis.

Finally, I would like to extend my appreciation to the faculty members of the Materials Science and Technology Master Program at Qatar University for the valuable lessons and knowledge they have imparted throughout my Master of Science studies. Their dedication and expertise have been instrumental in shaping my understanding and passion for the field of materials science and technology.

TABLE OF CONTENTS

LIST OF TABLES

LIST OF FIGURES

Chapter 1: Introduction

Nearly 17 years ago, the first results on multicomponent alloys were published.

The manipulation of configurational entropy and the expansion of the alloy composition realm enable a new level of control over solid solution phase stability in alloys. These two dissimilar concepts have captivated the attention of researchers in material science. High entropy alloy (HEA) is a term used a lot whenever scientists study multi-component elements in terms of their entropy. However, Miracle and Senkov (2017) suggest using the terms multi-principal element alloys (MPEAs) and complex, concentrated alloys (CCAs). These terms are suggested to be used whenever this field is described in general and to look into the uncharted territory of multi-component alloys. The intent is to alter the Nb content at various heat treatments in order to examine the microstructure, mechanical characteristics, and phase stability.

Alloys with high entropy encourage the development of intermetallic single-phase solid solutions. Hence phase identification steps are whether the phase is ordered or not, whether it is a solid solution or not, and whether it is a simple or complex phase. Many HEAs contain compound-forming elements like Al or Ti, resulting in unique microstructures. Despite the wide range of microstructures available, the HEA sector has grown to place a considerable focus on single-phase solid solutions. New research reveals that even microstructures with two intermetallic phases can provide an appealing balance of structural characteristics if the microstructure is carefully controlled. The use of intermetallic or ceramic phases in structural alloys, such as superalloys, is a deliberate and crucial aspect of the microstructure as they often make up a significant portion of the overall volume. Such alloys exhibit an exceptional combination of strength and high durability due to the careful control of the size, structure, size distribution, and allocation of intermetallic or ceramic phases (Miracle

et al., 2017).

Entropy-based alloys are characterized by the magnitude of entropy that alternates between low, medium, and high. For low entropy alloys, the ideal entropy value is less than 0.69R, while for medium entropy alloys, the ideal entropy value is within a range of 0.69R to 1.61R. For high entropy alloys, the ideal entropy value is greater than 1.61R. Scientists can easily calculate the entropy in an ideal solid solution from the alloy composition. However, it is important to note that the equation for calculating entropy assumes that atoms are in random lattice positions. The entropy of a system can be significantly affected by temperature, with high entropies typically observed at high temperatures or in the liquid state. However, it is important to note that binary metallic liquids do not possess atoms in random lattice positions, making them non-ideal (Miracle et al., 2017).

Lattice distortion plays a crucial role in solid solution hardening models and can contribute to an increase in configurational entropy. It can also make it challenging to identify the ordered and disordered phases using traditional X-ray diffraction techniques. The commonly used dendritic region (DR) parameter evaluates atom size fluctuation, but it may not accurately reflect structural distortion. The distortion of a solid solution can be reduced when larger atoms primarily occupy the first shell surrounding a smaller atom; thus, a method for measuring and modeling lattice distortions is crucial for a complete understanding of the properties of solid solutions. Therefore, a method for measuring and modeling lattice distortions is necessary to fully understand the properties of solid solutions.

A commonly observed alloy is the FeCrMnNiCo alloy, and after accounting for variations in grain size and strain rates, experimental results are in general agreement. This alloy typically exhibits a single-phase FCC solid solution microstructure, with the

exception of minor oxide, Cr-rich, or Mn-rich second-phase particles. Twins of coarse annealing are frequently encountered due to the crystal cooling (Yi et al., 2022). Over the whole temperature range, both yield and final strengths decrease with increasing temperature, as depicted in Figure 1. The decrease in strength is most significant when the temperature decreases from 77 Kelvin to 300 Kelvin, then it gradually decreases from 300 to 800 K, and the decrease becomes more noticeable at the highest test temperature. The ability of a material to stretch without breaking, known as tensile ductility, increases when the temperature is below 900 K. Dislocations might happen in the beginning at ($\varepsilon \leq 2.4\%$) by planar dislocation glide. However, when the temperature exceeds 300 K, and the plastic strain exceeds 20%, the planar character is lost, and the cell structure is reorganized.

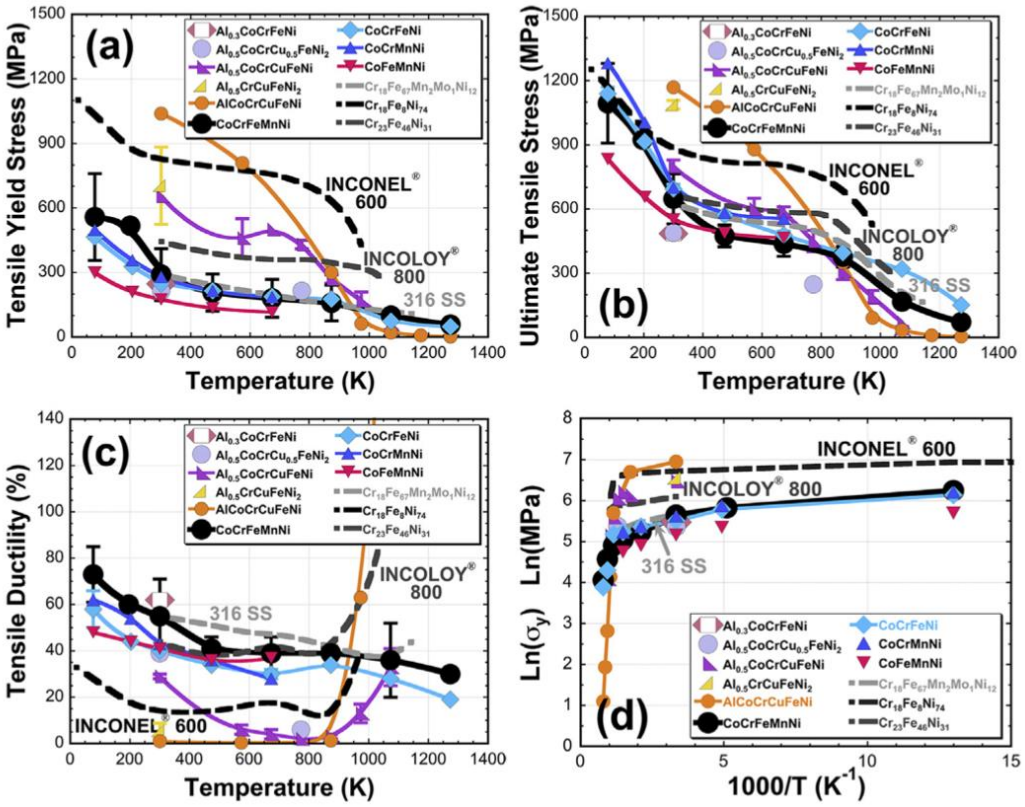

Figure 1: Tensile data of 3d transition metal CCAs

According to many research findings, it has been found in FeCrMnNiCo alloy, that all attempted elemental substitutions of Mn lessened the ideal solution property.

Moreover, this caused the formation of multi-phase alloys along with less entropy effect, toughness, and corrosion resistance. Therefore, this thesis aims to study the effect of Nb content at different heat treatments on the phase stability, mechanical properties, and microstructure of NiCoCrAl high entropy alloys.

The focus of this thesis is to investigate the following:

1. What stable phases could be formed by altering the Nb content in Ni0.55CoCrAlNbx high entropy alloys?
2. What are the corresponding mechanical properties as well as the evolved microstructure properties of the optimized single-phase high entropy alloys?

Chapter 2: Literature Review

Humans have continually sought to create new materials throughout history, and the development of new alloys has been a significant focus for over a decade (Hummel, 2004). This effort can be traced back to the bronze age when alloys were developed following a "base element" paradigm. While designing the alloys, the researchers previously paid attention to the phase diagram to improve the standard alloy that inhabits only a specific part of the phase design (George et al., 2019).

Most alloy development has focused on the selection of the main component, e.g., Fe, Al, Ni, etc., for its primary properties and adding additional elements to allow for secondary properties. A notable example of this is the Ni-based superalloys where Ni is the primary component for its favorable FCC structure, melting point, etc., and many other elements are added to control oxidation (Cr), solid solution strengthening (Mo, Co, Nb), and precipitation hardening (Al, Ti). The behavior of alloys with a single major component and, to a lesser extent, two or possibly three important components has been exhaustively studied for many decades. In recent years, multi-component alloys have been developed that can exhibit bulk glass formation and improved properties. (Takeuchi et al., 2012) provided detailed guidelines for their selection.

HEAs, or High Entropy Alloys, are a novel form of alloys made from multiple elements which are blended together in equiatomic concentrations, resulting in solid solutions. The following process goes into details of mixing more than five elements near- equiatomic ratios (Takeuchi et al., 2012). However, subsequent studies have indicated that multi-principal element alloys do not easily form solid solutions since enthalpy can often dominate the entropy effect. Recently, 130,000 alloy systems were studied by their phase diagrams and changes in temperature and microstructures (Senkov et al.,2017). According to the study, as the number of alloying elements in

solid solution alloys increases, they become less likely to form. As a result, previous understandings of disordered solid solution phases have been contradicted by increased entropy. There is a greater likelihood of intermetallic compounds being formed when there are more elements, even though entropy increases slightly as the number of elements increases. While it is now realized that simply adding more elements will not provide solid solution phases as guidance to experiment, it is still worthwhile to look at the earlier empirical rules of thumb.

Elements number of five and more mixing together are considered to be high entropy alloys. (Tsai & Yeh,2014). Altering the components of the mixture would result in different physical and chemical properties. The difference basically lies in solid solutions and compounds. According to Sheng's study (Tsai & Yeh,2014), if scientists could combine elements with a specified given composition, we can almost predict the type of phases (intermetallic phase, solid solution phase, or amorphous phase) a multi-component alloy design will form. This needs further development. However, this study was attracted to know the fundamental properties needed to predict phase stability. Hence, the research started by studying the high entropy alloys and focusing on statistically analyzing the elements' behavior. Studying the composition of elements in this research meant analyzing the different phases that form.

In contrast, Sheng got statistical records to compare them and figure out more information about amorphous phases or solid solution phases (Tsai & Yeh,2014). In this thesis, five parameters were used: the electronegativity difference (ΔX), the valence electron concentration (VEC), the atomic size difference (δ), the enthalpy of mixing (ΔH_{mix}), and the entropy of mixing (ΔS_{mix}). According to the data, the electronegativity difference (ΔX) would not influence the formation of phases. The VEC showed a minor effect on the formation of phases. The solid solution forms only when these three

parameters are met: ΔHmix, δ, and ΔSmix. The suitable range for atomic size difference is greater or equal to 0 and less or equal to 8.5. The suitable range for enthalpy of mixing is greater or equal to -22 kJ/mol and less or equal to 7 kJ/mol. The suitable range for the entropy of mixing is greater or equal to 11 J/(K·mol) and less or equal to 19.5 J/(K·mol). Nevertheless, the bulk metallic glasses form is limited to a certain range for the five parameters. On the other hand, the intermetallic phases form at transitional conditions in terms of the enthalpy of mixing, the entropy of mixing, and the atomic size difference. Whenever solid solution phases form, there is a possibility that intermetallic phase form but with less marginal glass. The analysis figured a specified range to form solid solutions. This specified range is whenever the atomic difference is kept lower than $\delta \leq 4.3$ while the entropy of mixing and enthalpy of mixing are left in the same range of solid solutions. Hence, choosing the right atomic size is crucial to determine the different phases to be established (Tsai & Yeh,2014).

The research conducted by Senkov et al. (2010) delved into the various families of complex concentrated alloys (CCA), with a specific focus on alloys containing 3d transition metals. One of the most commonly studied alloy families is made up of at least four of the following elements: aa. However, a new trend in alloy creation has emerged, where components are chosen to serve a specific purpose. Three distinct datasets were used to complete an extensive microstructural examination: two sets of computed data generated by CALPHAD created from 408 alloys with unique. All group concentrates on distinct elements and present diverse microstructural patterns. The combined proportions of the component crystal organizations in each dataset are utilized in a (SISO) analysis applied here to predict trends across these three datasets. Altogether, thirteen single-phase fields of multi-principal elements were exposed by this microstructural analysis. The contributions of Al, Cr, and Cu are examined in order

to uncover the relationship between properties of 3D transition metal, microstructure, composition and Multi-Principal Element Alloys. After a thorough assessment, certain Industrial stainless steels, alloy steels, and particular functional substances, all of which have three or more major components, are identified as MPEAs. Moreover, refractory metal CCAs have the capability to amplify the strength and/or temperature of nickel superalloys, Despite the fact that commercial stainless steel austenitic and alloy steels and third-generation transition metal CCAs have similar mechanical qualities (Zhang et al., 2008). Two main HEA hypotheses may be addressed thanks to detailed studies of microstructures and characteristics of Senkov et al. ,2010). Despite not being supported by evidence, the entropy "effect" has had a lasting effect by raising awareness of the importance of structural entropy in processability. Data do not support the sluggish diffusion idea, but it forces us to reconsider a key idea about metallic diffusion. As a result of recently released research, the CCA field has expanded to cover materials having ionic, metallic, or covalent bonding. (Miracle & Senkov ,2017). Included are microstructures with any quantity and type of phases. Finally, it is demonstrated that structural and functional materials applications are included in the MPEA field. Many future initiatives are suggested, with a focus on creating high-throughput structural material tests and calculations. The HEA field hasn't lost any of its power and continues to raise new issues and provide new opportunities. Future research will be motivated by the wide variety of complicated compositions and microstructures.

Ye et al. (2016) asserted that the new paradigm for HEA alloy synthesis essentially entails mixing a number of elements in an equimolar composition. Canter et. al (2004) referred to these designed multicomponent alloys as HEAs, meaning that the configurational entropy of the component random mixing in these alloys is high. More and more study is being done on HEAs, and it has been discovered that alloys

with the same amount of elements may have different configuration entropies for mixing (Smix). In the past, equation 1 made it simple to determine the entropy of mixing for HEA.

$$\Delta S_{mix} = R \ln n \qquad \text{(EQ.1) (Tsai\& Yeh,2014)}$$

n is the total number of the constituent elements, and R is the gas constant. (Tsai& Yeh,2014)

Interestingly, under room temperature HEAs don't just undergo the solid solutions phases, but also intermetallic compounds and metallic glasses. Zhang et al. (2016) proposed the use of two new parameters, δ and the enthalpy of mixing ΔH_{mix}, in place of ΔSmix for analyzing alloys at low temperatures because ΔSmix alone is not sufficient.

$$\delta\% = 100\% \sqrt{\sum_{i=1}^{n} ci \left(1 - \frac{ri}{\sum_{j=1}^{n} c_j r_i}\right)^2} \qquad \text{(EQ.2)}$$

$$\Delta\text{Hmix} = \sum_{i=1, i\neq j}^{n} \Omega_{ij} c_j c_i = \sum_{i=1, i\neq j}^{n} 4\Delta H_{ij}^{mix} c_j c_i \qquad \text{(EQ.3)}$$

The atomic radius and atomic fractions c_j and c_i are the atomic fractions. Solid solutions are usually produced under atomic size difference and low enthalpy of mixing, which falls into this range -15kJ/mol < ΔHmix < 5 kJ/mol and 0< δ <5.

The Elemental Composition of HEAs:

A study or a deeper understanding was focused on the multi-component alloys to understand their structure and properties of the crystalline phase (Cantor et al.,2004). The authors tested equiatomic multi-component alloys with various elements by casting and melt spinning. Utilizing , X-ray diffractometry, electron microscopy, electron probe microanalysis, and microhardness, the following characteristics were investigated.. The results showed that equiatomic alloys that contain sixteen and twenty constituents are brittle and multiphase crystalline. This was true for both methods: melt

spinning and casting. A single FCC solid solution was produced from a five-component alloy.. The same phase transition happened to different alloys of six to nine components; however, it dissolved many of the transition metals. Germanium and Copper are more electronegative elements, making them less stable, pushing them into interdendritic (ID) areas. The number of phases is lower than the Gibbs phase rule's highest optimal equilibrium number. Additionally, the number of phases is less than what is permitted for non-equilibrium solidification. No metallic glasses were spun or cast from the multicomponent alloys. The Hume-Rothery Rule states that since the difference in atomic radius between each component is less than 15%, a solid solution should form (Cantor et al.,2004).

Ye et al. (2016) claim that whenever scientists wanted to create a specific alloy, they concentrated on the phase diagram's corners. However, the emphasis shifted to the central region with the advent of high entropy alloys. Interestingly, as the multiple principal elements develop fundamental challenges, it faces theories, methods for conventional alloys, and models. It could be difficult to identify the optimal alloy compositions using the conventional method of trial-and-error. Thus, a high-through put alloy screening method is needed. This method worked not only on conventional methods but also on high-entropy alloys. The HEAs showed features of specific strength, superconductivity, exceptional mechanical performance, super para magnetism, and exceptional ductility. The stated assets guarantee great future inventions and equipment improvements. For instance, some aluminum HEAs alloys are utilized in energy sectors and the transportation industry because they acquire the property of being very lightweight. HEAs containing Niobium, Molybdenum, and Tantalum remain brittle at T>1200 ºC (Ye et al., 2016).

In Hou, Hui, and Yao et al. (2019) paper, a high entropy alloy was put in to

experiment to improve its properties using the presence of the element Boron. It was previously studied by Seol et al. (2018), that adding boron to equiatomic and non equiatomic Fe20Mn20Cr20Co20Ni20 can increase the yield strength by greater than 100%. Contrary to it, the ductile strength is enhanced to about 40% more than before. This assures scientists that mechanical properties are being transformed greatly due to the addition of boron. The properties are varied with boron because the slightest composition of this element alters the grain boundary's structure, energy, and composition. Despite this, another study made by Zhang et al. (2008) in an attempt to add boron to the composition of BCC AlFeCoCrNi. After analyzing the mechanical properties, FCC, mass borides and bulk borides appeared. This means the boron did not enhance the properties; instead, the properties have deteriorated poorly. Hence, Hou et al. (2019) prepared AlFeCoNi integrated with boron to investigate the optimum composition where characteristics are greatly improved.

Chanda and Das conducted a study in 2017 to investigate the impact of adding the element Niobium (Nb) to a Co-rich high entropy alloy on phase development, stability, microstructure refinement, and mechanical characteristics. They hypothesized that Nb addition would destabilize the FCC phase and could lead to severe lattice distortion but ultimately hoped to strengthen the phases in CoCrFeNi. The microstructure results showed changes in the alloy depending on the amount of Nb added, with the formation of thin nano lamellar FCC-Ni and HCP Fe2Nb-type Laves phases. The alloy with the highest amount of Nb, x=0.5, had a high yield strength of 2060 MPa and showed significant plasticity and strain hardening. Transmission electron microscopy examinations discovered that the movement of displacements played a role in the high yield strength and ductility seen in the eutectic FCC/Laves lamellae and at their interface.

Cantor and colleagues in 2004, studied the phase behavior of transition metal alloys that form a single FCC phase. They found that alloys composed of 16 or 20 components were multiphase, crystalline, and brittle, but a five-component alloy (Fe20 Cr20 Mn20 Ni20 Co20) solidified as a single FCC solid solution. Additionally, the study found that large quantities of other transition metals such as Ti, V and Nb can be dissolved in other 6 to 9-component late transition metal-rich multi-component alloys. They also found that elements like Cu and Ge, which are more electronegative, are less stable in the FCC dendrites and tend to reject into the inter-dendritic areas. The total number of phases present in the alloy was always substantially lower than the maximum number expected by the Gibbs phase rule and even lower than the maximum number under non-equilibrium solidification circumstances. The study also found that casting or melt spinning late transition metal abundant multicomponent alloys does not produce glassy structures, which suggests that other variables are more significant in encouraging glass development.

Structural Stability of HEAs:

Guo and Liu (2011) talked about the phase stability in alloys with high entropy. By examining the vacuum electron concentration, atomic size difference, enthalpy of mixing, electronegativity, and entropy of mixing, the research primarily examined the amorphous phase and solid formation. They statistically built a database of HEAs to determine the fundamental concept behind phase stability. According to a study by Zhang and his team in 2014, for an alloy to form a solid solution, the difference in atomic size between the elements must be small, and the energy needed to mix them should be positive. On the other hand, the atomic size difference must be big for an alloy to form a bulk metallic glass, and the energy needed to mix them must be negative. Based on these findings, Guo and his team did an experiment; they found out that the amount of energy needed to mix elements is not the only factor that determines if an

alloy will form a solid or not. They determined that for a solid solution, the difference in atomic size should be between 0 to 8.5 and the energy needed to mix them should be between -22 to 7 kJ/mol, and the amount of entropy should be between 11 to 19.5 J/(K•mol). As for the bulk metallic glass, the difference in atomic size must be greater than 9, the energy needed to mix them should be between -49 to -5.5 kJ/mol, and the amount of entropy should be between 7 to 16 J/(K•mol).

According to Nong et al. (2020), HEA alloys are discussed many times in terms of mixing different elements and analyzing certain parameters. However, few studies are focused on the stability of the alloys synthesized. Hence, Nong et al.(2020) conducted an evaluation of $Al_{0.5}CrCuFeMnTi$ to study the solid solution stability and its impact on bonding and the structure of the alloy. To do so, the result focused on measuring the energies and the bonding of the phase structure composed. The cast $Al_{0.5}CrCuFeMnTi$ HEA alloy presents a dendritic morphology in the DR region. The following elements were depicted a lot in the DR region: iron, chromium and titanium. At the same time, copper was richer in the interdendritic (ID) region. This can be explained because iron, chromium, and titanium have a large enthalpy of mixing with copper. This hinders the copper from going to the dendritic region ID. Between the DR and ID there was an interface noticed where chaotic arrangements of atoms are found. The stability is studied from the phases using Broyden–Fletcher–Goldfarb–Shanno. The X-ray diffraction measurements showed that the structure of the C14 and BCC crystal lattices was enlarged, which is consistent with the findings. The stability of the DR phase is primarily due to the strong covalent bond between the elements iron, aluminum, titanium, and chromium. Additionally, the covalent bond between aluminum, copper, and manganese is particularly strong in the ID phase. The conditions of atomic size and enthalpy of mixing were met. The results complied with the ranges,

but for the dendritic phase, the atomic size was larger than the requirements; however, the enthalpy is reduced, which stabilities the distortion of the lattice.

Wu et al. (2015) noted that despite the majority of materials, they typically show a reciprocal temperature-dependence of ductility and strength. But the FCC FeNiCrCoMn HEA exhibits simultaneous increases in elasticity and strength at low temperatures (from 293 to 77 K). Nanoscaled mechanical twinning was discovered during deformation at a low temperature of 77 K. These deformation modes may improve fracture toughness, uniform elongation, and strain hardening. This behaviour can be seen in low-number-element alloys like 5-element FeNiCrCoMn alloys, 4-element equiatomic FeNiCrCo alloys, and even 3-element equiatomic NiCoCr alloys. Single crystals of a multi-component equiatomic FeNiCoCr alloy with FCC structure were produced for mechanical analysis to assist in understanding the fundamental deformation phenomena of compositionally complex alloys. Chen et al. (2021) found that despite the fact that this material exhibits slip in a standard FCC manner at temperatures of 293 and 77 K, its high-temperature sensitivity is exceptional compared to other FCC metals. They also mention that there are many limitations to HEAs, such as the fact that the strength of FeCoNiCrMn with a single-phase FCC structure is typically considered insufficient. Additionally, the alloy WNbMoTaV with a BCC structure lacks tensile ductility. Additionally, HEAs' low castability and compositional segregation restrict their uses. Lots of methods are suggested to resolve this, such as adjusting Mn concentrations in non-equiatomic Fe40Mn40Co10Cr10. Deng et al. were able to change the deformation process from dislocation glide to twin deformation, achieving incredible strength and ductility at the same time. Vacuum arc melting and suction casting were used to compose TixAlCoCrFeNi2.1(x = 0, 0.1, 0.5, 0.2). Later, a curve of tensile stress-strain was studied. Microstructures show a morphological change

from lamellae to petal with the addition of Ti, resulting in a dual phase of B2 and L12. It has been confirmed that there is a strict K-S OR between the lamellar microstructures 111FCC/011B2 and 011>FCC/111>B2, whereas the petal-like microstructure deviates from this phase orientation relationship. In the Ti0.15AlCoCrFeNi2.1 alloy, the B2 matrix and Cr-rich nanoparticles with a variety of morphologies are coherent. As Ti concentration rises, ultimate tensile strength and elongation first increase before declining until 3.17 at. percent (x = 0.2) Ti addition. The balance of the L12 and B2 phases and the precipitation of Cr-rich nanoparticles contribute to the alloy's good mix of the ultimate tensile strength (1253 MPa) and ductility (12.9%) in the as-cast state.

According to Jiang et al. (2021), single-phased FCC is often ductile but not sufficiently strong, which is why eutectic HEAs exist. However, single-phase BCC-constructed HEAs may be extremely robust yet fragile. Such alloys, which often have poor castability and compositional segregation, cannot be used in industrial applications. In order to improve fluidity and castability and eliminate the strength-ductility trade-off, Lu et al. developed and produced eutectic HEAs. In this study, a novel Al0.9CoFeNi2 eutectic high entropy alloy's microstructures and deformation characteristics were examined (EHEA). The dual-phase lamellar eutectic bulk cast Al0.9CoFeNi2 EHEA microstructure has an order face-centered cubic FCC (L12) and an order body-centered cubic FCC (L13) (B2). The FCC (L12) and B2 phases' volume fractions were found to be 60% and 40%, respectively. At room temperature, the hard B2 phase was combined with the ductile, soft FCC (L12) phase, producing a material with improved strength of 1005 MPa and elasticity of 6.2 percent in tension. The Al0.9CoFeNi2 EHEA showed excellent work hardening capabilities and three phases of work hardening. Planar slips are prevalent in both the B2 phase and the FCC (L12) phase. The forming dislocation substructures undergoing uniaxial tensile deformation indicate that the FCC (L12)

phase is easier to deform than the B2 phase. According to post-deformation transmission electron microscopy, the sub-structural evolution of the FCC (L12) phase progresses from planar dislocations to bending dislocations, high-density dislocations, dislocation networks, dislocation walls, and Taylor lattices, whereas the sub-structural evolution of the B2 phase progresses from a few short dislocations to numerous planar dislocations. Additionally, a brittle-like fracture in the B2 phase and an apparent ductile fracture in the FCC (L12) phase were present on the fracture surface of the Al0.9CoFeNi2 EHEA.

As mentioned deformation twinning (DT) is very critical in affecting high entropy alloys. The presence of DT can increase the ductility and strength of the HEAs. In the research of Park and Kim (2020), boundary twining behavior gets further studied. They conducted tensile testings on a high entropy alloy CoCrFeMnNi. These testings included an isothermal and two-stage nonisothermal. The results obtained showed that at a temperature of 500°C, the two-stage tensile testing showed high flow stress of around 90 to 120 MPa. This could be clarified by the twining mechanism. In the pre-existing secondary twin boundaries of twin lamellae grains, local deformation was observed approximately 0.5 mm away from the fracture point of the two-stage tensile specimen. The region around this area featured a high concentration of deformation twins and ultra-fine grains. It appears that the formation of ultra-fine grains is the result of local deformation-induced grain fragmentation followed by rotational recrystallization.

Processing Techniques of HEAs

In Hou, Hui and Yao et al. (2019) paper, they prepared AlFeCoNi integrated with boron as previously mentioned. The aim here is to find the composition where both FCC and BCC are present to get the required objective in upgrading the properties.

The alloy AlFeCoNiBx was created using vacuum arc melting equipment by Hou et al. with varying boron compositions of x=0, x=0.05, x=10, x=15 and x=0.2. The process was performed under a pressure of 10-1 Pa while the valve was opened and 3.0 x 10 -3 Pa when the valve was closed, in order to purify the argon gas to 99.99%. The melting of the arc began at a pressure of 6.0 x 10 -2 Pa and the alloy was kept in the furnace under the same pressure for purification.

Nong et al. (2020) prepared a cast $Al_{0.5}$CrCuFeMnTi HEA alloy. The synthesize of the HEA alloy had the following composition: x_{Al}=0.5, x_{Cr}=1, x_{Cu}=1, x_{Fe}=1, x_{Mn}=1 and x_{Ti}= 1. The furnace used was called ZKYI vacuum arc under argon protection acquiring high purity. The alloy was remelted four times to be certain that the composition is uniform. The high vacuum was 0.5 x10 -4 Pa in the furnace after the evacuation. Later, the cast is obtained and cooled by a water-cooled copper crucible. A different apparatus was used to extract data about the crystal structure, microstructure, and composition of $Al_{0.5}$CrCuFeMnTi.

Like other synthesizes, the cast of $Al_{0.7}CoCrFeNiTi_{0.3}$ alloy Zhong et al. (2021) was prepared in a vacuum arc melting furnace with a purity of metals higher than 99.95%. However, their alloy was melted and cooled around five times to ensure the blending of composition. The SEM, TEM, XRD, and EDS apparatus were used to evaluate the alloy in terms of microstructure, fracture, morphology, and crystal structure. Three phases are found in crystal structure: $L2_1$, FCC, and BCC. The $L2_1$ had a constant of 5.832 Å. The FCC had a constant of 3.596 Å.

Cieslak et al. (2018) studied AlxFeNiCrCo experimentally (HEA) to complement previous findings (which confirmed phase coexistence in Al-Fe-Ni-Cr-Co HEA systems). An alternate technique is used to make alloy samples based on the sintering of pure metallic powders and arc-melting. Series were prepared, each having

different aluminum content varying from x=0 to x=1.5. The first series SM1 is melted under argon gas in an arc-melting furnace. For the uniformity of elements, it was remelted 4 times. The cooling was very fast, from 1400 °C to room temperature in approximately one minute. SM2 was conducted in a very similar way but annealed at 1000°C for seventy-two hours in a vacuum of 6 x 10^{-6} mbar. As for the SS3 series, it was done by sintering metallic powders mixed. They were compressed under a pressure of 3 x 10 8 Pa. It was annealed for two weeks (one day at 500 °C the other day at 1000 °C). The researchers used X-ray and neutron diffraction to study the structural characteristics of the HEA samples, allowing them to identify the crystal structures and their contributions. They also employed electron microscopic techniques to determine the phase compositions. The results from these methods were found to be similar, with the BCC/B2 and FCC phases being the dominant ones. Within these two structures, three phases with varying stoichiometries were discovered and their presence, composition, and impact on the HEA were found to be influenced by the Al content. When comparing the sintered and melted samples, it was observed that although the phase composition of the AlxFe-NiCrCo alloys was similar, the microstructures were vastly different, with the melted samples displaying a dendritic structure and the sintered samples showing large regular grains.

Microstructures of HEAs

Cabibbo et al. (2020) state that adding Nb to HEAs (particularly 5-element HEAs) enhances the ductility and strength of the alloy. The atomic radius of Nb is larger than the other elements in the alloy, such as Co, Fe, Cr, and Ni. This results in negative mixing enthalpies when combined with these elements, leading to the formation of Nb-enriched Laves phases. Laves phases have a hexagonal close-packed (hcp) crystalline structure, which greatly enhances properties such as yield strength, fracture strength,

and elastic modulus as they precipitate within the face-centered cubic (FCC) matrix, as demonstrated in Figure 2. In this research, an equiatomic CoCrFeNiNb high-entropy alloy was created using a series of conventional induction melting, compaction by spark plasma sintering, and powder metallurgy. The high-entropy alloy's microstructure was made up of a combination of an FCC solid solution reinforced by a hcp Laves phase, which forms due to Nb's larger atomic radius compared to the other elements and negative mixing enthalpies with Co, Fe, Cr, and Ni. As the quantity of Nb increases, the volume fraction of Laves phases increases, which diminishes alloy plasticity. The as-cast HEA's had an ultimate compression strength (UCS) of 1400 MPa, which increased to 2400 MPa following sintering and compaction at 1273 K. The experimental UCS was found to have a good agreement.

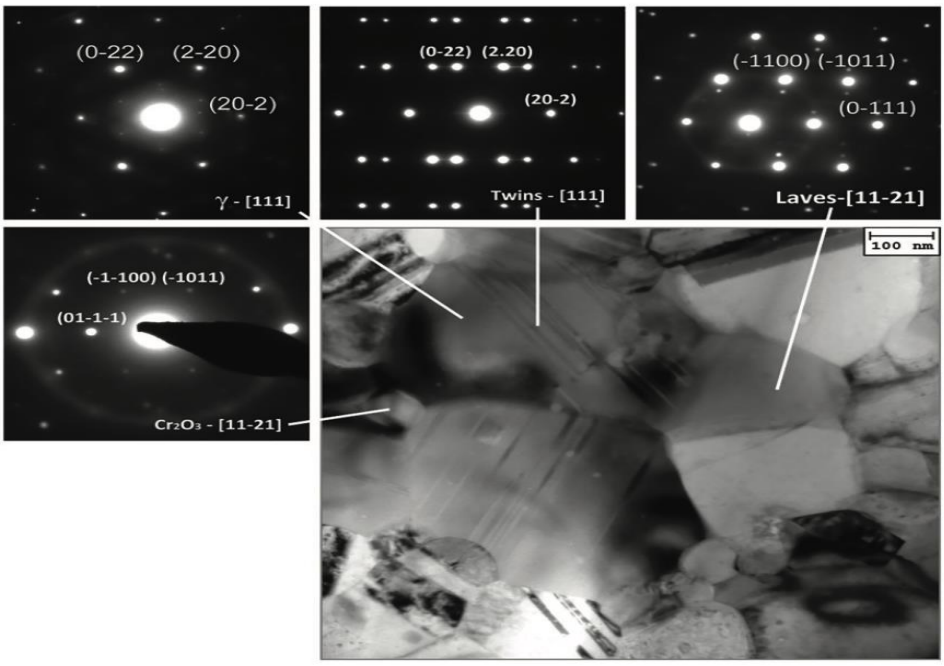

Figure 2: Transmission electron microscopy micrographs of the 8h MA+SPS alloy compacted at 1273 K.

Note. Adapted from "Compression stress strengthening modeling of an ultrafine-grained equiatomic SPS CoCrFeNiNb high-entropy alloy.," by M. Cabibbo Průša, F., Šenková, A., Školáková, A., Kučera, V., & Veselka, Z., 2020, Proceedings of the Institution of Mechanical Engineers, Part C: Journal of Mechanical Engineering Science, 235(8), p.1432-1442 (https://doi.org/10.1177/0954406220943245).

According to Shao et al., HEAs with a single FCC step, like CoCuFeNiMn, have drawn increased interest because of their outstanding mechanical properties at both high and low temperatures (2020). These HEAs are constructed of FCC, BCC, and hexagonally close-packed (HCP) phases in a single-stage structure. Despite its high ductility at room temperature, its low yield strength (of roughly 300 MPa) keeps it from being widely used. The backscattered electron (BSE) mode microstructure of (CoCuFeNi)100-xMox (x = 0, 10, 15, 19, and 25) HEAs is depicted in Figure 3. HEAs have been strengthened using a single phase employing techniques like grain refining, second phase strengthening, strain strengthening, and others. One of the most popular ways to enhance an alloy's mechanical properties is by adding additional components. The development of a second phase and lattice deformation may be triggered by alloy constituents, including Hf, Nb, V, Zr, and others, which may impede dislocation migration in HEAs. Vacuum arc melting was used to create high entropy (CoCuFeNi)100-xMox (x = 0, 10, 15, 19, and 25 values in atomic ratio) alloys to demonstrate how the inclusion of Mo affects the microstructure and mechanical properties. The results showed that a phase formed and significant separation took place when Mo was added to the high entropy alloys. The content of the phase expanded as Mo content increased. The microstructure of the alloys changed from a single-phase face-center-cubic (FCC) solid solution structure at x = 0 to a hypoeutectic microstructure at x = 15, a fully eutectic architecture at x = 19, and finally, a hyper eutectic microstructure at x = 25. It was found that the phase and FCC phases interact coherently. The maximum yield strength and fracture strength of the (CoCuFeNi)81Mo19 alloy with fully eutectic microstructures in tensile testing at room temperature was 557 MPa and 767 MPa, respectively. According to the fracture surface, the phase's formation in substantial amounts caused the (CoCuFeNi)100-xMox alloys

to lose their ductility.

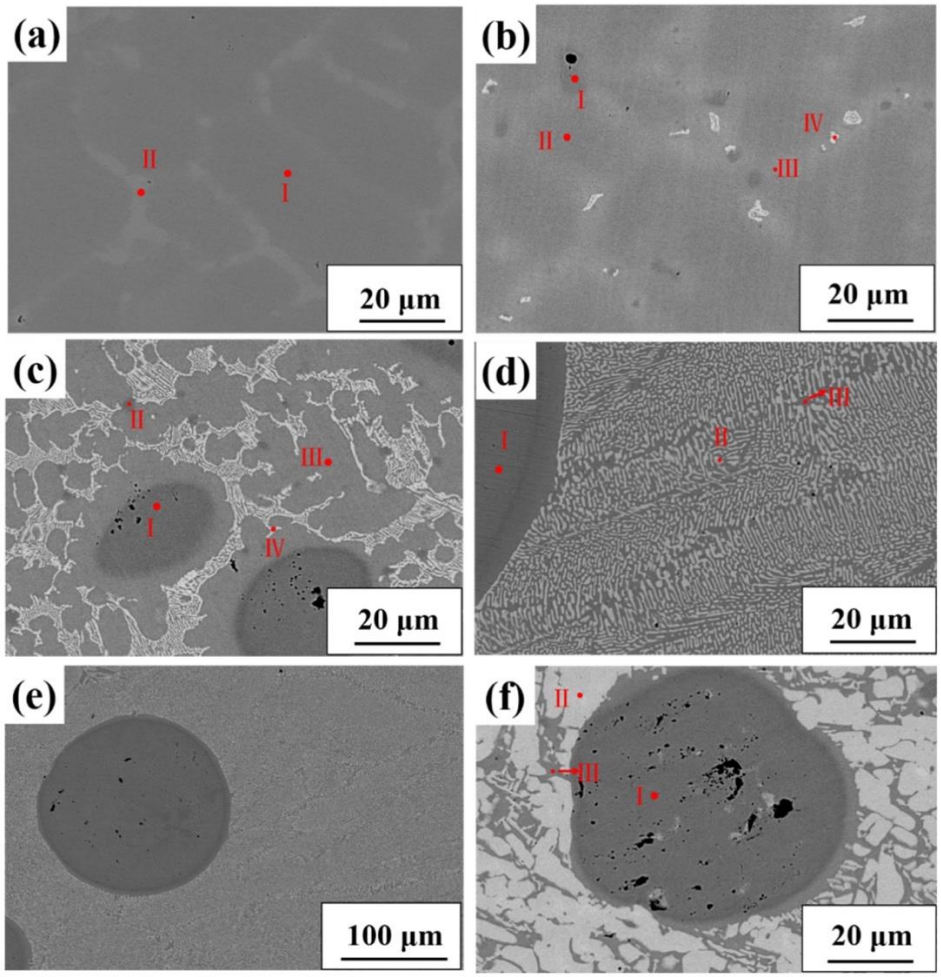

Figure 3: Effect of mo addition on the microstructure of $(CoCuFeNi)_{100-x}Mo_x$ HEAs

Note. Adapted from "Effect of mo addition on the microstructure and mechanical properties of CoCuFeNi high entropy alloy," by Shao, Y., Ma, H., & Wang, Y., 2020, *Metals*, *10*(8), p.1017 (https://doi.org/10.3390/met10081017). Copyright statement.

Pra et al. (2020) used standard induction melting, mechanical alloying for eight hours, and spark plasma sintering to compact an equiatomic CoCrFeNiNb alloy. The mechanically alloyed alloy was composed of an FCC solid solution with reinforcement from HCP Laves phases, and it exhibited a uniform ultrafine-grained microstructure. A thorough TEM inspection revealed the presence of nanocrystalline Cr2O3 particles at the triple junctions of the present grains as well as stacking faults and nanotwins, which

were largely discovered inside the FCC solid solution grains. The alloy has an as-cast hardness of 648+18 HV 30 and a final compressive strength of 1374 MPa. An even greater hardness of 798+9 HV 30 and extremely high strengths of 2412 MPa were present in the mechanically alloyed alloy that was compressed at 1000 degrees C. The previous strength estimate was found to be in excellent agreement with results from microstructure strengthening modeling, which revealed a calculated mean value of 2300 MPa, based on TEM quantitative analyses that examined the influence of numerous structural elements and lattice flaws. Additionally, the mechanically alloyed alloy showed exceptional thermal stability as it kept its strength of 2284 MPa and hardness of 777 5 HV 30 even after extensive annealing/testing at 600°C.

Mechanical Properties of High Entropy Alloys

The HEAs have potential applications in a number of industries, including magnetic materials, cutters, and moulds. Strength and ductility are balanced in HEAs' dual-phase structures. The CoCrFeNi2Al1-xWx alloys were evaluated in Dong and Lu's study (2019). With 45% compressive loads, the results revealed that there was no breakage. Instead, a break was discovered while inspecting the lateral surface. Other alloy samples examined did not exhibit any cracking at a 50% strain. On the lateral surface, there are no visible cracks either. Therefore, it is obvious from this that an increase in the percentage of FCC phases caused a steady drop in the alloys' x values, yield strength, and hardness. Additionally, the hardness was decreased as a result of the declining BCC phase %. The alloy demonstrated better yield strength and hardness when compared to the single-phase face cubic crystal HEAs. Thus, Al and W element concentration can be adjusted and altered to provide the best mechanical qualities of strength and ductility.

In Hou, Hui, and Yao et al. (2019) synthesize of AlFeCoNi integrated with

boron, the microstructure, chemical composition, grain size, and crystal structure were measured via different equipment. LabX XRD-6000X-ray diffraction and JEOL JXA-8100 electron probe microanalyzer measurements illustrated that the FCC phase formed as soon as the slightest content was added from the boron. Moreover, the solubility of boron was depicted in the B2 matrix. Furthermore, as the content of boron kept on increasing, dendrites were arising. The eutectic structure and B2 phase were reached in the secondary stage. First, the phase of B2 is converted to both B2 phase and particle FCC; then, the eutectic structure and the B2 phase are established. Note that when the content of boron was 0.15, the eutectic structure was the finest, as the grain size was measured to be the smallest. However, as the content was further increased, the grain size of the eutectic structure and B2 phase was shown to be increasing. The impact of composition on mechanical characteristics. The yield strength increased from 805 MPa to 1253 MPa results due to a solid solution strength inclining. The fine grain strengthening also contributed to an increase in yield strength and fracture structural strength. The flexibility increased as soon as the eutectic structure was created from a strip of FCC1 and FCC2. As the boron level grew from 0 to 0.2, the plastic strain increased from 0.07 to 0.27. It may be inferred from the calculations that the alloy AlFeCoNiB0.15 had the best composition, with boron at a concentration of 0.15. No bromides were noticed in this stud, revealings that there is the possibility that the γ conditions cannot tell the phases of the alloy.

Zhong et al. (2021) investigated $Al_{0.7}CoCrFeNiTi_{0.3}$ alloy to find the right composition that will obtain strength and plasticity. The excellent mixture of strength and ductility can only be designed by eutectic high entropy alloy. This was proposed just after learning that the single phases of FCC or BCC do not result in the required properties. As stated before, 3 phases are found in crystal structure: $L2_1$, FCC, BCC.

The dendritic structure was noticed with both the interdendritic (ID) and dendritic region (DR). The DR mainly has the FCC phase, while both ID and DR. The DR mainly has FCC phase while ID has $L2_1$ and BCC. The alloy's composition of the element is very comparable to the BCC. But $L2_1$ phase has more composition of the elements: aluminum, titanium, and nickel. Regarding the FCC phase, it contained a lot of chromium and iron. One of the best qualities was discovered to be the mechanical properties. Together with a fracture strength estimated to be 2990 MPa, the yield strength is 1438 MPa. The compressive plasticity is 37.7% towards the end. The alloy's composite integrated phases, including the hard BCC/L21 phase and the soft FCC phase, have improved plasticity by more than 30%.

Youssef et al. (2014) suggested lowering the stacking fault energy for 4 alloys (equiatomic NiFeCrCoMn, equiatomic NiFeCrCo, non-equiatomic $Ni_{14}Fe_{20}Cr_{26}Co_{20}Mn_{20}$ and non-equiatomic $Ni_{18.5}Fe_{18.5}Cr_{18.5}Co_{26}Mn_{18.5}$) to see its effect on the mechanical properties. However, low SFE causes dislocation cross-slip with wide spaces. The deformation twins induce higher strength and ductility, which is the study's objective. The results showed no major impacts on the properties after lowering SFE. The alloy results showed comparable features with steel that has twinning plasticity. The thermal stability for $Ni_{14}Fe_{20}Cr_{26}Co_{20}Mn_{20}$ was very low as it was forming σ-phase particles when annealed at a temperature less than 1100°C. It must be noted that the presence of the element cobalt increased the elongation by 30%. Yet that is not significant since yield strength was reduced. Interestingly the equiatomic NiFeCrCo alloy in fine, coarse samples illustrated superior measurements in ductility and strength. 80% higher toughness. This is due to its high strain hardening exponent.

As noted by Detrois et al. (2019), the increasing demands for efficiency and power

output in power plants have led to the need for new materials that can withstand high temperatures. An important factor in the design of these systems is the ability to operate at elevated temperatures, which is often limited by the temperature capabilities of the materials used. In order to meet these demands, materials with exceptional mechanical and thermodynamic properties are in high demand. Superalloys based on nickel and cobalt-reinforced superalloys have historically been crucial in developing components exposed to high pressure and temperature. These alloys have a face-centered cubic (FCC) crystal structure matrix seamlessly integrated into a microstructure characterized by (Ni3Al) precipitates with an ordered L12 crystal structure. In order to study the phase stability across a range of compositions in the Al-Co-Cr-Fe-Nb-Ni system, six high-entropy alloys with non-equiatomic compositions were created. Analysis was conducted using SEM, TEM, and XRD, with the assistance of computational methods, to compare the results to the experimental findings. It was found that exposure to 900°C led to the formation of Laves, NiAl, and other phases, resulting in complex microstructures. As the concentration of Fe and Nb increased, the primary and secondary Laves populations stabilized. Additionally, the presence of Nb resulted in the growth of a thin, plate-like phase at the expense of the secondary Laves phases. It was also discovered that alloys with a high Fe concentration precipitate the NiAl phase above the solvus temperature. Overall, the phase composition predictions made by thermodynamic calculations using the TCNi8 database were accurate, and the phase stability predictions made by TTNi8 were outstanding. However, the solvus temperatures of the precipitate stages varied significantly. Al (20) Li (20) Mg (10) Sc (20) Ti (30), a low-density, nanocrystalline, high-entropy alloy, was produced by Youssef et al. (2014) through yet another mechanical alloying. It produced a single-phase FCC arrangement during ball milling, which after one hour of annealing at 500°C

transformed into a single-phase hcp structure. The alloy is significantly stronger than other alloys and has a strength-to-weight ratio that is comparable to ceramics. The material created by mechanical alloying that didn't have a lot of N, O impurities had a single-phase FCC crystal structure. Its nanocrystalline particles were about 12 nanometers in size. This sample's lattice parameter was measured to be 0.4323 nm. This sample had an extremely high mechanical hardness of 5.8 GPa. The nanocrystalline grain sizes of these alloys contribute to their great mechanical toughness.

According to Senkov et al. (2010), the need for metallic alloys with superior mechanical and functional properties is still quite high in the aerospace industry. Conventional alloys are frequently considered to be an established technology, especially for structural applications. The chemistry of such alloys is typically dominated by a base element, which makes up 80% (by weight) or more of the total composition. Even superalloys, which can contain up to 12 elements in one alloy, frequently have a base element content of more than 50%. Only a few cases of superalloys with up to 20% of each of up to three transition metal elements (Fe, Ni, Co, and/or Cr) have been created. The alloying approach is restricted because in multicomponent alloys, ternary or more complex intermetallic compounds tend to appear unexpectedly, especially when exposed to high operating temperatures for a long time. These novel stages often feature intricate crystal structures which prevent flexibility and scavenge valuable components from the host phase. Mechanical characteristics, corrosion resistance, and microstructure stability are all reduced when these complex intermetallics form. Vacuum arc melting was used to make Two refractory high-entropy alloys with nearly equal atomic concentrations are W-Nb-Mo-Ta and W-Nb-Mo-Ta-V. Despite the presence of a significant number of elements, both

alloys have a single-phase body-centered cubic (BCC) structure. The lattice parameters a=3.2134(3) for the quaternary alloy and a=3.1832(3) for the quaternary alloy were determined using high-energy X-ray diffraction and a scattering vector length range of 0.7 to 20 A1. In comparison to the W-Nb-Mo-Ta-V alloy, which had a density of r12 12.36 g/cm3 and a Vickers microhardness of Hv 14 5250 MPa, the W-Nb-Mo-Ta alloy had a Vickers microhardness of Hv 14 4455 MPa. The extraordinary microhardness of these alloys exceeds that of any individual component, implying that a solid-solution-like strengthening process is complicated alloy composition.

In brief, the previous studies examined different variations of high entropy alloys. The element selection part in the investigation alters the components of the mixture would result in different physical and chemical properties. The composition of the high entropy alloy $Ni_{0.55}CoCrAlNb_x$ has not been investigated in any of the papers reviewed. Therefore, the aim of the thesis is to fill the gap by providing information about $Ni_{0.55}CoCrAlNb_x$ HEA. Hence, an analysis is done to this new mixture by varying the composition under specific heat treatment.

Chapter 3: Methodology

Materials and Methods

Bulk-size pieces of nickel, cobalt, chromium, aluminum, and niobium were used to produce $Ni_xCoCrAlNb_{x-1,}$ the samples of alloy. Four different alloys were investigated by varying the Niobium composition along with Nickel. Using the glove box under argon gas, shown in figure 4, the elements were weighed according to $Ni_{0.55}CoCrAlNb_x$ formula and then put into a stainless-steel vial. The vial is loaded into the argon tube with a pressure gauge 5 x 10^{-2} mbar.

Figure 4: glove box under argon gas

Then the alloy was smelted by MAM1 (D-72379 Hechingen by Edmund Buhler) vacuum arc furnace, shown in figure 5. The starting voltage in the arc melting is 2 V. this voltage is used to melt titanium to remove moisture and any oxygen traces. In the beginning, the arc melter was evacuated to a pressure value of 2×10^{-3} bar and then refilled with an ultra-purity (UHP) argon gas. This process was repeated at least three times to ensure an inert atmosphere before the melting process. Finally, the arc melting process of the alloy was conducted. Each alloy was remelted five times and cooled down in the arc melter.

Figure 5: MAM1 (D-72379 Hechingen by Edmund Buhler) vacuum arc

To ensure uniform compositions in the high entropy alloys, the samples were annealed in a tube furnace (GSL-1500X – RTP50 - MTI corporation). The annealing process was conducted under an inert UHP argon atmosphere. The HEA samples are annealed at a temperature of 1000°C for 48 hours. The inert argon gas was purged in the furnace tube after applying a high vacuum (5×10^{-6} bar) using a turbo pump purge HiCUBE (PFEIFFER) presented in Figure 6.

Figure 6: pump purge HiCUBE (PFEIFFER).

The experiment is divided into two methods: Diamond Saw and rolling. In the Low-

Speed Diamond Saw SYJ-150 (MTI corporation), shown in figure 7, the alloy was cut into small discs.

Figure 7:Diamond Saw SYJ-150 (MTI corporation)

In the Rolling Mills (Durston) shown in figure 8, the $Ni_{0.55}CoCrAlNb_x$ alloy samples were cold-rolled to improve the strength characteristics of the HEA alloy.

Figure 8: The rolling mill used to roll the samples during thermomechanical treatment.

Characterization

To analyze the $Ni_{0.55}CoCrAlNb_x$ alloy samples, a characterization technique is used to certify whether the purpose of the proposal is met or not. In the material science field, there are many techniques to measure and study the microstructure, stability, and mechanical properties of the high entropy alloy. This characterization section states the procedures and approaches implemented in this study.

Mechanical Properties Characterization

Vickers Microhardness (HV).

A tool used to gauge a material's hardness is the microhardness tester. Vickers Microhardness (Future-Tech, FM-ARS900) was utilized in this study to measure hardness with a 10-second dwell duration. For each sample, a measurement was made using 25gf and eight indentations for milled and annealed powders. As seen in figure 9, this device works by using a cubic trapezium diamond indenter to create indentions on the surface of the material while applying a particular amount of force and time. The following equation is used to calculate hardness based on the depth of these indentations: F: applied force, d: is the average length of the indent diagonal.

$$HV = \frac{0.1854\ F(kg)}{d_{avr}^2(mm^2)}$$

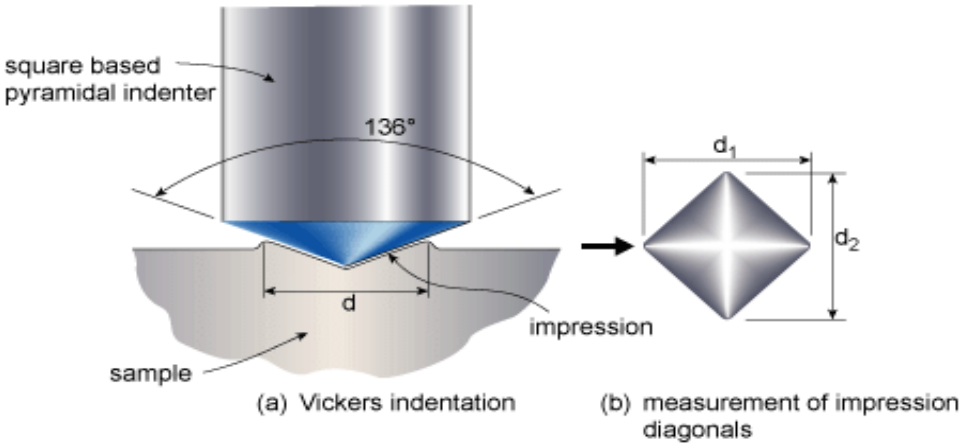

Figure 9: Vickers Microhardness (HV)

Tensile Tests.

In the tensile test, a sample is clamped into grips. The material's dimensions, such as length and cross-sectional area, are measured before analysis. Moreover, a cutter (Pocket NC), displayed in figure 10, is used to cut the sample to specific dimensions - in the same rolling direction done in the Rolling Mill. Then the load is applied to the material at the two fixed ends by a tensile machine (MTESTQuattro). A continuous increase of the weight, known as the load, while monitoring the change in length of the sample. The pulling at the ends continues until the sample breaks. This breaking could extract lots of data about the strength and mechanical behavior of material. A graph is usually depicted plotting engineering stress versus engineering strain.

Figure 10: A miniturized tensile machine (MTESTQuattro).

Structural Characterization

X-Ray Diffraction (XRD).

The most frequent use is to analyze crystalline samples to determine their crystal structure. XRD is a tool for analysis that uses X-ray beams to determine the crystal structure of metallic or ionic crystals. This method can also determine the average distance between atom layers, gauge the size of a sample's grains, and measure the strain caused by deformation in a material. An X-ray emitter, a sample holder, and a detector are the three main parts of the XRD apparatus, as depicted in figure 11. The

sample causes an incoming ray from the X-ray source to be diffracted by an angle equal to the angles of the original two beams. Additionally, depending on the separations between atomic planes, the diffraction of an X-Ray as it passes through a crystal happens at various angles. On the sensor plate, black spots are created when the contact surfaces are in phase (constructive). The radius of concentric spheres created by sample rotation is used to calculate the separation between plates inside the crystal structure. Based on the ray intensities, XRD can be used to extract a diffractogram. The size of the unit cell can be determined from the result data by computing the distance (d) between adjacent layers in a crystal.

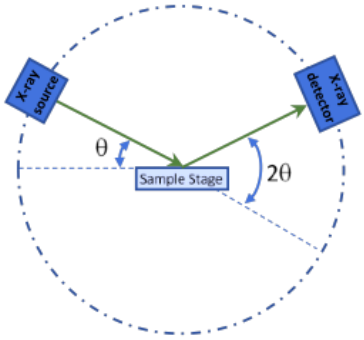

Figure 11: Illustration of XRD equipment components

Braggs Law is a computed formula for the relationship between X-ray beam wavelength and d, which is given by:

$$\lambda = 2d\,sin\theta$$

where θ is the incident angle that falls between the X-ray beam and the surface of the crystal. In figure 12, a representation of Braggs law is shown. Diffraction occurs when an angle satisfies Braggs Law.

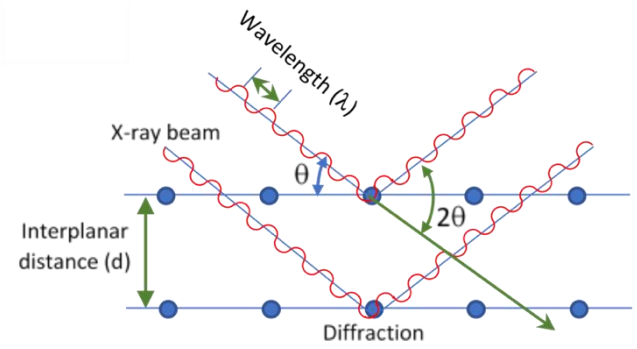

Figure 12: Representation of Braggs law angle diffraction

Furthermore, particle size and crystalline strain within the unit cell may be calculated from the peaks of an XRD diffractogram. The idea that material processing affects peak breadth and intensity is the foundation of several proposed hypotheses. Below is a description of the two-grain size computation models used in this study. According to the Williamson-Hall approach, the strain is constant in all crystallographic orientations, and the widening brought on by grain size and strain is additive to the Bragg's peak that is created. The resulting equation is as follows:

$$\beta_{hkl} \cos\theta = \left(\frac{k\lambda}{D}\right) + (4\,\varepsilon \sin\theta)$$

where, k is a constant, ε is the strain, D is the grain size, β_{hkl} is the width of the peak at the half-maximum intensity.

A linear graph of data from peaks of a vs. plot produces a slope. As shown in Figure 13, the slope represents the strain value and the y-intercept of a constant divided by the interplanar distance.

In order to learn about particle size and strain, the Warren-Averbach method describes diffraction peaks using the Fourier series. As a result, we obtain the following equation by combining the Cauchy and Gaussian functions:

$$\frac{{\beta_{hkl}}^2}{\tan^2\theta} = \frac{\lambda}{D}\left(\frac{\beta_{hkl}}{\tan\theta \sin\theta}\right) + 25\,\langle\varepsilon^2\rangle$$

The relationship between a sample's grain size, strain, and peak width can be plotted on

a linear graph. The x-axis represents the value of $\frac{\beta_{hkl}{}^2}{\tan^2\theta}$) and the y-axis represents the value of $\left(\frac{\beta_{hkl}}{\tan\theta\,\sin\theta}\right)$.. The slope of this graph represents a constant multiplied by the square of the strain value, and the y-intercept represents a constant divided by the interplanar spacing.

Scanning Electron Microscope (SEM)

SEM is used to examine a material's topography and surface geometry. The equipment consists of a sample inlet chamber that operates under a vacuum atmosphere.

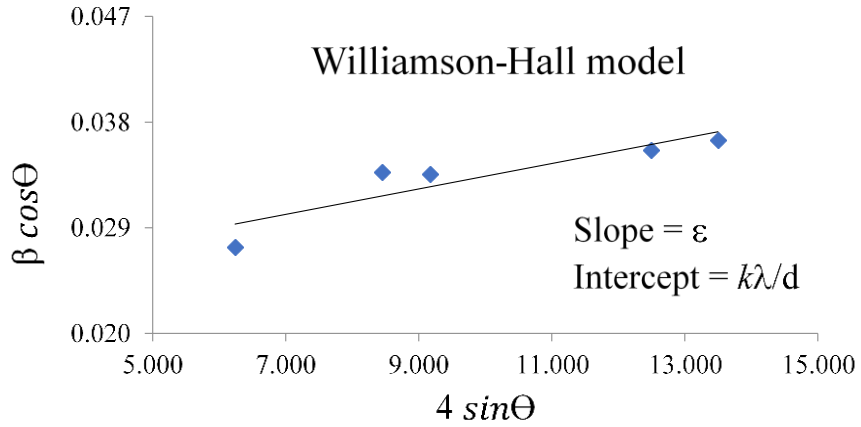

Figure 13: Warren-Averbach approach linear graph

The electrons are generated from an electron source (electron gun) located at the top of the microscope's column. The entire sample is scanned from every angle as the electron beam moves through the tungsten bulb and through the vacuum-sealed chamber. Depending on how they interact with the beam, the sample's electrons emit in a variety

of ways. Figure 14 illustrates an SEM diagram that shows the main contents.

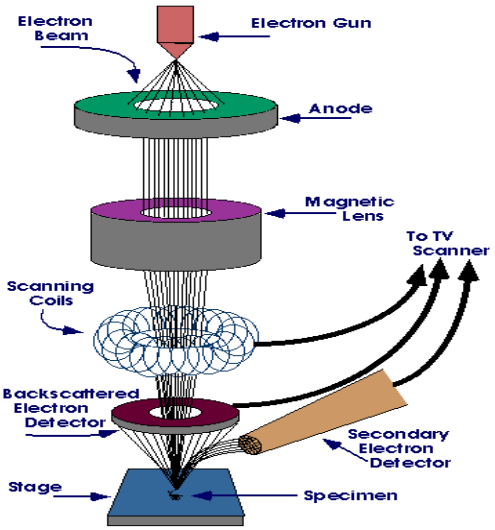

Figure 14: Image of Scanning Electron Microscope

For microstructure analysis, polishing was done for the samples by Gender-Polisher (FORCIPOL2V-Metkon) shown in figure 15. Then itching is done by damping it in an etchant (acid) for 40 seconds. The acid is a mixture solution- hydrochloric acid HCl 5ml, acetic acid CH_3COOH 10ml, and Cupric sulfate $CuSO_4$ 1g. After that, the ingot is washed with running water for five minutes and then observed under an optical microscope (BX53MTRF-S-Olympus).

Figure 15: Image of the Polisher (FORCIPOL2V-Metkon)

Purpose of Characterization

The alloy $Ni_{0.55}CoCrAlNb_x$ is analyzed in three different sections. First, the HEAs were cut into using diamond saw discs, and then the characterizations technique was used. Then cold rolling is used to roll the HEAs at different reduction percentages. After that, the cold rolled samples were aged under an inert atmosphere in a tube furnace for one hour at 600°C, 800°C, 950°C and 1000°C. The steps indicated above represent the thermomechanical treatments depicted in this thesis. Then the microstructure, phase analysis, and mechanical properties of the samples were evaluated. Not just that, the microstructure was continuously studied after finalizing the discs. The study included many devices: XRD, SEM, tensile, and HV to observe the best sample that achieved the optimum features in mechanical and microstructure.

All the characterization techniques helped in finding the optimum composition of the alloy $Ni_{0.55}CoCrAlNb_x$. In addition, the machines helped in studying; further, the behaviors resulting from varying the concentrations of the elements. The purpose of the research is fulfilled by gaining more knowledge about structural stability, bonding characterization, and high-strengths. The $Ni_{0.55}CoCrAlNb_x$ alloy was prepared in three samples with different amounts of Nb: 0%, 1%, 3%, and 5%. Then for each sample, multiple analyses were made to determine the phase stability and mechanical properties. The analysis was divided into annealing samples, cold rolling of the sample, and rolling the sample with aging at different temperatures in a furnace for one hour. In table 1, a scheme for the flow of data that will be presented in this research is explained.

Table 1: Scheme for the flow of data

$Ni_{0.55}CoCrAlNb_x$ alloy was prepared in Four samples:		
SAMPLE 1- $Ni_{0.55}Co_{0.3}Cr_{0.1}Al_{0.05}Nb_0$ alloy		
SAMPLE 2- $Ni_{0.54}Co_{0.3}Cr_{0.1}Al_{0.05}Nb_{0.01}$ alloy		
SAMPLE 3- $Ni_{0.52}Co_{0.3}Cr_{0.1}Al_{0.05}Nb_{0.03}$ alloy		
SAMPLE 4- $Ni_{0.50}Co_{0.3}Cr_{0.1}Al_{0.05}Nb_{0.05}$ alloy		
Sample cut to Discs *annealed*	**Sample is cold rolled**	**Sample is rolled and aged** *at 600°C, 800°C, 950°C and 1000°C for 1 hour*
Conducted Tests	**Conducted Tests**	**Conducted Tests**
XRD	XRD	XRD
Microhardness	Microhardness	Microhardness
Tensile Test	Tensile Test	Tensile Test
Microstructure	Microstructure	Microstructure
SEM	SEM	SEM

Note that after retrieving the data for the 5% sample under annealing, cold-rolling, and aging at different temperatures for 1 hour, the results were satisfactory in choosing the best condition for the HEA. Hence, it has been decided to proceed with the study of samples: 0%, 1%, and 3 % by only analyzing the characteristics under aging at 950°C for 1 hour.

Chapter 4: Results And Discussion

This thesis describes how to make the high entropy alloys NiCoCrAlNbx (x = 0, 0.01, 0.03, and 0.05) by vacuum arc melting. The chemical makeup of the alloys examined for this thesis is shown in Table 2. The systematic review of the recrystallization of the Ni-based alloys served as the basis for the selection of the subsequent annealing settings for the ingots produced after arc melting (Coyne-Grell et al., 2022). All of the ingots

were annealed for 48 hours at 1000°C in a tube furnace using an ultra-high purity (UHP) Argon environment. Following room-temperature air cooling, the samples underwent a cold rolling process without any heat treatment. The aging of HEAs containing 5% Nb was carried out at various degrees of 600°C, 800°C, 950°C, and 1000°C for an hour under UHP Argon in order to comprehend the recrystallization mechanism and optimize the aging conditions methodically. On the HEA5 alloy (5% Nb), the aging conditions were optimized to achieve the optimal balance of strength and ductility. Then, in these ideal conditions, a comparison of structural and mechanical characteristics as a function of the Nb content was examined. On all the HEAs under consideration, thorough structural analysis and mechanical property evaluations were carried out.

Table 2: Chemical compositions of the HEAs under investigation $NiCoCrAlNb_x$ (x= 0, 0.01, 0.03, and 0.05)

Sample	Composition (at.%)				
	Ni	Co	Cr	Al	Nb
HEA0	55%	30%	10%	5%	0%
HEA1	54%	30%	10%	5%	1%
HEA3	52%	30%	10%	5%	3%
HEA5	50%	30%	10%	5%	5%

Selection of the Elements

The high entropy alloys NiCoCrAlNbx are chosen in this thesis for a thorough analysis that is centered on the elemental performance in earlier research. Khan et al. (2022) claim that Stacking Fault Energy (SFE) is a characteristic that directly affects an alloy's plastic deformation mechanism. A number of alloys were created to evaluate their SFE, and the results showed that Ni increased the SFE. Another study discovered that a decrease in SFE was associated with an increase in Co. As a result, when Ni and Co interact, there is a positive and negative cancellation effect.

According to Chanda and Das (2017), the addition of Nb to arc-melted CoCrFeNiNbx (0.45x0.65) high entropy alloys produced alloys with a higher hardness value of 521 HV and a significant increase in ductility of 17%. Hence, based on these studies, it is predicted that the mixture of $NiCoCrAlNb_x$ alloy would end with high hardness and deformation that would make the alloy applicable to be used in advanced structural applications. In Kirk et al. investigation (2022), the high entropy alloy was analyzed to have low melting points whenever Ni was replaced. This is a crucial concern to take in mind in manufacturing a sought-after product. Thus, the HEAs in this study contain Ni to ensure a relatively high melting point. According to Vazquez et al. (2022), Nb as transitional metal is expected to have high yield strength. This is directly related to the elemental quantities of electronegativity variance (X_{var}), atomic-size differences (δ), and formation enthalpy (E_{form}). Their prediction matched the results in the experiments, and they emphasized that phase stability and excellent mechanical properties are not necessarily the outcome of high chemical entropy or valence electron count.

Heat Treatment Analysis of HEA5

Microstructure of HEA5 at different heat treatments.

The microstructures of the HEA5 alloy under various aging treatment conditions are depicted in Figure 14. In Figure 14a, the HEA5 sample that was heated to 600°C is displayed. It is important to note that the annealed sample's microstructure revealed relatively large grain sizes in the 220 mm range. The annealed sample was cold rolled with a 60% reduction, which caused the plastic deformation, which caused the grains to lengthen in the rolling direction with a higher density of dislocations and shear bands. As shown in Fig. 14a, the cold-rolled sample's microstructure was unaffected by aging at 600°C for one hour. The microstructure of the elongated grains contains a

comparatively high density of shear bands. According to Fig. 14b, the sample's microstructure exhibits characteristics similar to those of samples aged at 600°C and showed sheer bands and dislocations. Fig. 14c depicts the microstructure of the aged HEA5 sample after it was heated to 950°C for an hour. The deformed structure of the cold-rolled sample is completely recrystallized with a grain size that is substantially smaller than that of the annealed sample, as can be seen in the micrograph. The aged sample at 950°C has an average grain size of about 45 m. Additionally, second-phase precipitation was seen in Fig. 14c at the HEA5's grain boundaries. After aging at relatively high temperatures, second-phase precipitation is anticipated, especially in alloy systems with multiple alloying elements. Other reports with different alloy compositions have reported seeing precipitation [He et al. (2016 ; 2017); Wang et al. (2022)]. The crystalline structure of the HEA5 specimen aged at 1000°C for one hour is depicted in Figure 14d. The micrograph shows that the grain size increases over that of the sample that has been aged at 950°C. It is discovered that the typical grain size is 110 m. The micrograph also shows that after aging at 1000°C, an increased concentration of annealing twins developed in the microstructure. Due to the relatively low SFE of such an alloy and the presence of elements like Co and Nb, annealing twins, as seen in Fig. 14d, would form. The second-phase precipitations are also seen in Fig. 14d to be preserved in the microstructure after this specimen.

Masemola et al. (2020) concluded in their investigation of AlCrMnFeNi alloy that as the annealing temperature increased from 400°C to 1000°C the grains began to coarsen. Another report by Gu et al. (2019) indicated that annealing temperatures decide whether a partial or full recrystallization structure is formed. From our results, it appears that the temperature of 950°C could be considered the recrystallization temperature for this alloy composition.

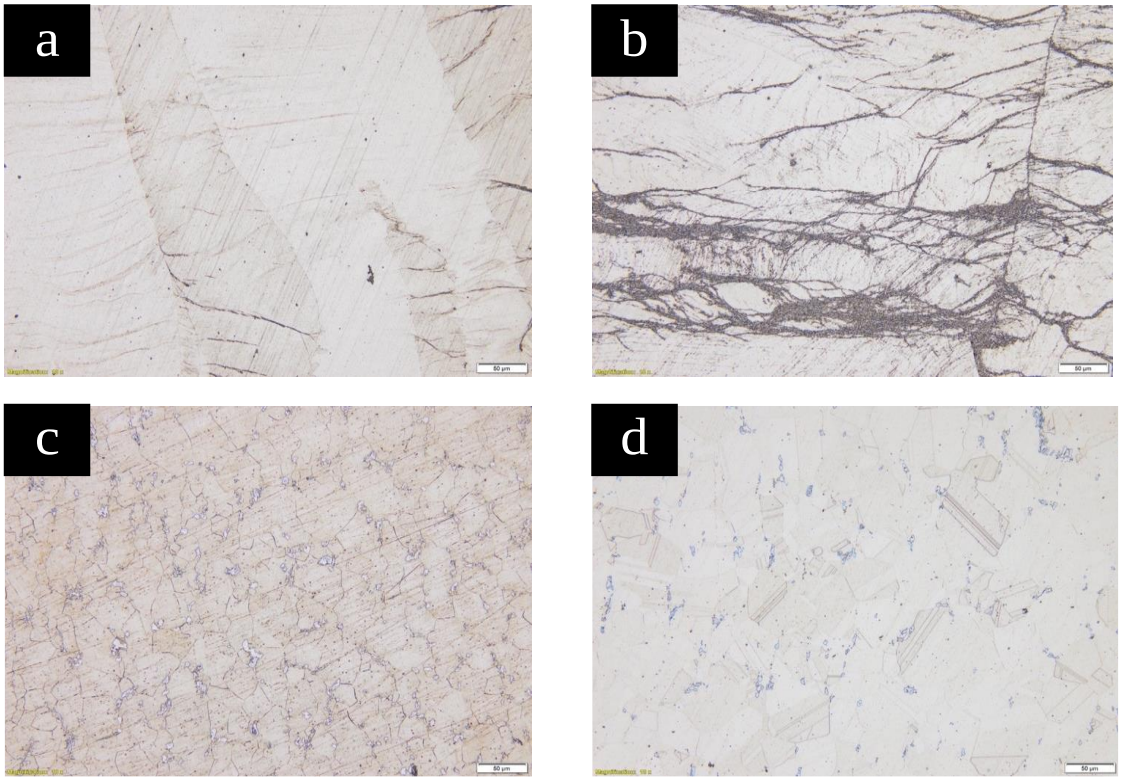

Figure 16: Microstructure of the aged HEA5 at different temperatures: (a) 600°C, (b) 800°C, (c) 950°C, and (d) 1000°C.

X-Ray diffraction of HEA5 with different heat treatment.

The aged samples were subjected to XRD analysis in order to determine the phases that resulted from the various aging conditions. The x-ray diffraction patterns of the HEA5 alloy at various aging temperatures are shown in Figure 15. Figure 15 demonstrates that an FCC solid solution is the primary phase that developed in all of the samples aged at various temperatures. In their investigation of the Ni0.46Cr0.23Co0.23Al0.4Ti0.4, Lu et al. (2020) discovered that the XRD analysis showed the formation of a single-phase FCC crystalline structure over time.

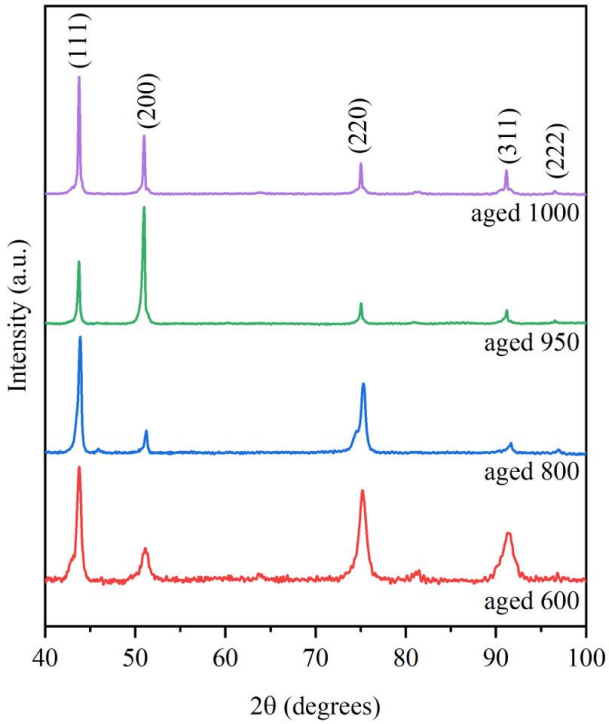

Figure 17: XRD patterns of the HEA5 at different aging temperatures.

Mechanical Properties of HEA5 at Different Heat Treatments

The hardness of HEA5 at different heat treatment.

For the microhardness measurements, a load value of 25gf at a dwelling time of 10 seconds has been done eight times to investigate the repeatability of measurements for all the samples investigated in this research. Figure 16 represents the microhardness of the HEA5 samples at different aging conditions. The sample that was cold rolled has

the highest hardness, measuring 7.02 GPa. The high dislocation density produced by cold rolling may be the cause of this incredibly high microhardness. The dislocation density gradually decreases with increasing temperature for the aged samples, and the microhardness slowly reduces due to the recovery process. The microhardness of the samples aged at 600°C and 800°C decreased to values of 6.87 GPa and 5.2 GPa, illustrating that the recovery process primarily occurs at relatively low temperatures (Figure 16). The sample maintained its microhardness value of 4.69 GPa after aging at 950°C without experiencing a discernible loss in strength. This could be related to the recrystallization process, which yielded a relatively small grain size and also the precipitation of the second phase at the grain boundaries (see Fig. 14c). The microhardness of the sample aged at 1000°C is decreased to a value of 4.43 GPa. The decrease in hardness value in this sample could be attributed to the observed grain growth at this aging temperature (see Fig. 14d). This behavior is constant with the research reported by Masemola et al. (2020), which observed that grain growth could contribute to decreasing in hardness. Another explanation is made by researchers Miracle and Senkov (2017) that as the annealing temperature is further raised this produces an increase in the volume fraction occupied by atoms in Face Centered Cubic cell; consequently, the hardness is decreased. Besides, soft FCC phases also play a role in this decrease in hardness.

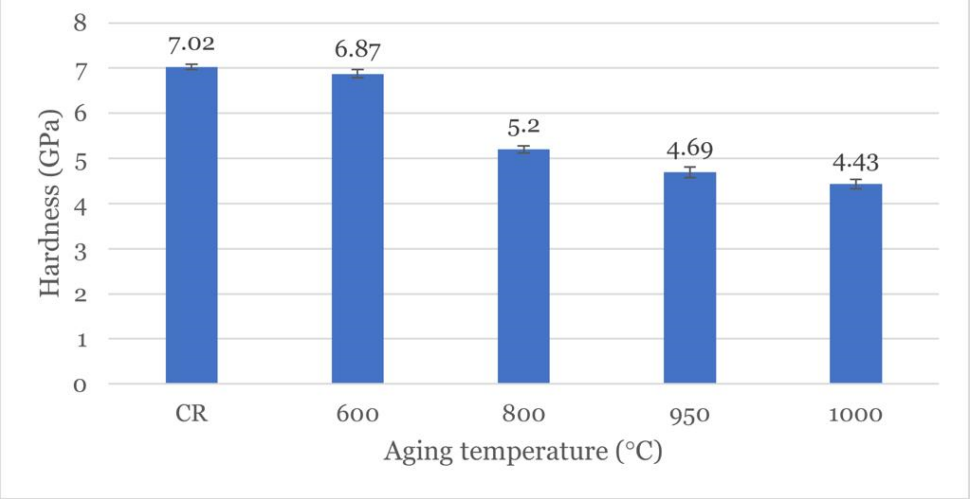

Figure 18: A bar graph comparison of microhardness and the different treated temperatures of HEA5

Tensile properties of HEA5 at different heat treatments.

Tensile testing was used to examine the HEA5 sample's intricate mechanical behavior. The test was run at room temperature with a 1×10^{-3} s^{-1} strain rate. Each sample underwent three tests to ensure that the outcomes could be repeated. For the HEA5 samples aged at various temperatures, Figure 17 displays the engineering stress-strain curves. The annealed HEA5 alloy displayed a uniform elongation of 31% and a yield strength of 850 MPa. Al0.45CoCrFeNi high-entropy alloy is annealed in Hou et al. (2019) 's paper, where it gains an elongation of almost 15% and a yield strength of 1000 MPa. The difference in annealing temperatures is what causes this variation in elongation. While Hou et al. (2019) paper's is annealed at 800°C, HEA5 is annealed at 2000°C. Similarly, raising the aging temperature above 800°C significantly improved the ductility of the HEA5 alloy. At a stress of 1840 MPa, the aged HEA sample displayed brittle behavior and experienced an early fracture. The high dislocation density produced in the microstructure after cold rolling and aging at such a low temperature may be responsible for this high strength (see Figure 14a). The sample exhibits limited ductile behavior with extraordinarily high yield and maximum tensile strengths when the aging temperature is raised to 800 °C. The sample aged at 800°C

had yield and maximum strength strengths of 1650 and 1795 MPa, respectively. This incredibly high strength is unheard of in alloy compositions of this type. At 800 °C, the alloy uniformly elongates by 2.5%, and the overall elongation is close to 4%. The microstructure results, which show that the dislocation density decreases as the aging temperature rises, help to make sense of the findings (see Fig. 14).

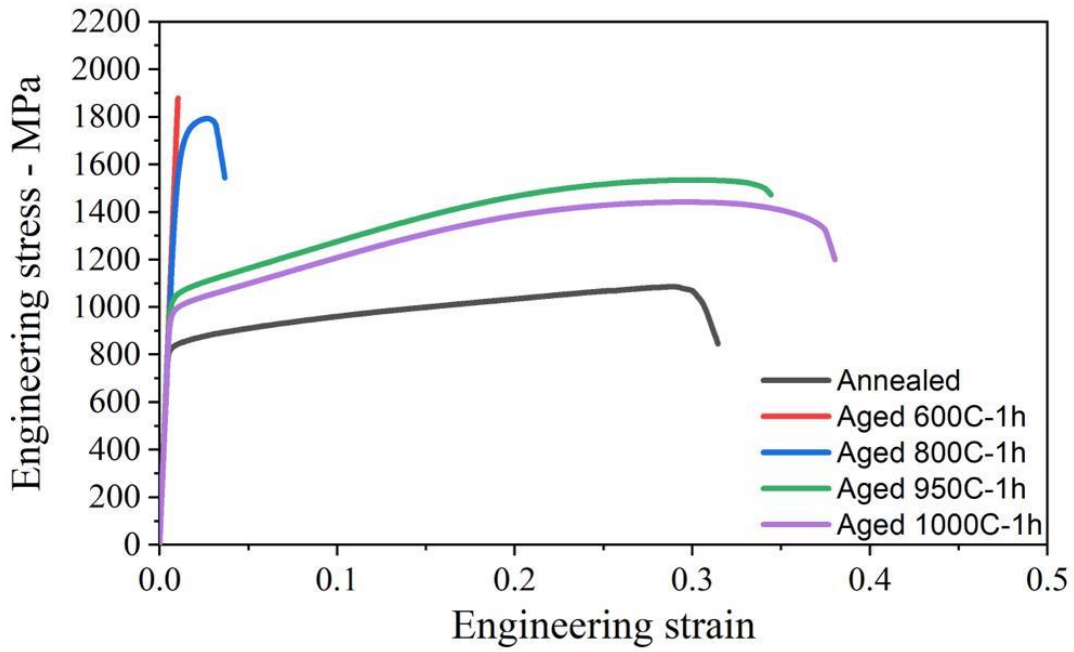

Figure 19: The engineering stress-strain curves of the HEA5 at different aging conditions.

The alloy's ductility was greatly improved by raising the aging temperature above 800°C. The samples aged at 950°C and 1000°C displayed a total elongation of 34% and 38%, as shown in Fig. 17. As shown in Figures 14c and 14d, the creation of recrystallized grains is what causes this advancement in ductility. Large grains that have been fully recrystallized would enable the dislocations in this alloy's FCC structure to slide.

The older samples at 950°C and 1000°C have yield strengths of 1050 MPa and 1000 MPa, respectively. The aged samples' elongation at 950°C and 1000°C samples were estimated to be 34% and 38%, respectively. Due to the occurrence of recrystallization, this ductility symbolizes the elastic properties of samples, which is considerably higher than the prepared samples. Among all the heat-treated samples, the features of the aged specimen at 950°C showed the best balance of strength and ductility. As a result, throughout the thesis, this condition will be implemented in the remaining samples with numerous Nb contents. According to Hou et al. (2019), annealing with different heat treatment temperatures showed variations in mechanical properties. The elongation of the AlNiCoFeCr alloy they studied increased as the heat treatment temperature intensified from 700°C to 1100°C. This is comparable to the elongation results obtained in our study and shown in the stress-strain curve, Figure 17. Hereafter, a direct relationship between heat treatment temperature and the ductility of HEA's materials could be observed. In another investigation on a high entropy alloy AlCrFeMnNi, Masemola et al. (2020) observed that as the aging temperature increased above 400°C, the soft and ductile characteristics of the FCC phase started forming. The samples' yield strength was also significantly reduced at temperatures below 800 °C, proving that excessive annealing is not always beneficial. According to our study's findings, the yield strength drops while the ductility improves as the temperature is elevated above 950°C, indicating that excessive annealing may not be beneficial.

Fracture surface analysis of HEA5 at different heat treatments

Figure 18 shows the fracture surface of the HEA5 samples after tensile testing, which were aged at 800°C, 950°C, and 1000°C. The fracture surface of the HEA5 aged at 800°C shows a combination of brittle and ductile fracture surfaces (Fig. 18a). The small presence of the dimples and microvoids indicates a limited extent of ductility, which is

shown in the tensile stress-strain curve, Fig 17. However, the fracture surfaces of the samples aged at 950°C and 1000°C indicate ductile behavior after tensile testing (Figures 18b and c). This is illustrated by the high density and large size of the microvoids in the dimpled structure. The results confirm the observed high ductility of these two samples. This is constant with the outcomes obtained by Masemola et al. (2020), Zhu et al. (2017), and Cai et al. (2022).

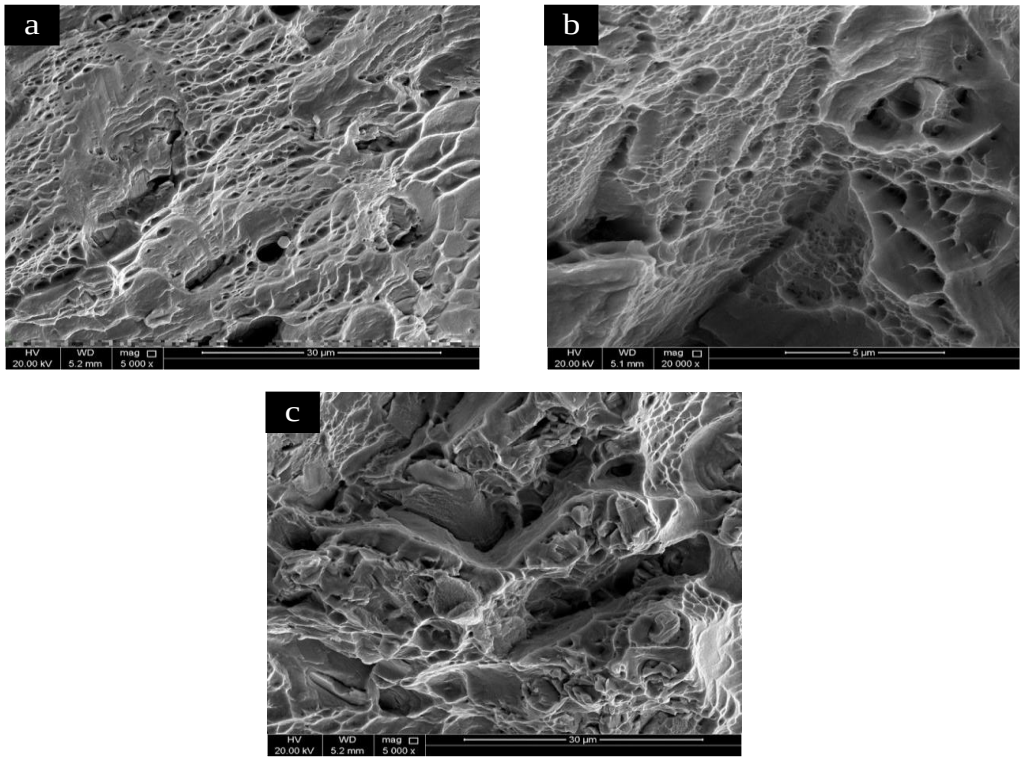

Figure 20: High magnification SEM BSE images of as-cast HEA5 alloys aged at different temperatures: (a) 800°C, (b) 950°C, and (c) 1000°C.

HEA5 samples treated at various temperatures were compared based on the analysis results in order to achieve the best phase precipitation, recrystallization, mechanical properties, and tensile elongation. According to the micro-structural results, the treated sample's grain size at 950°C has a size of 45 μm. However, grain growth was observed as the temperature rose to 1000°C. Additionally, the subsequent tests using optical microscopy and XRD showed that aging at 950°C results in the FCC phase fully

recrystallizing. The samples' microhardness was examined, and it was discovered that the sample aged at 950°C had a harder surface than the sample aged at 1000°C. The sample showed the best balance of strength and ductility at 950°C when the tensile test was also conducted. The yield strength is 1050 MPa, the ultimate tensile strength is 1534 MPa at 950 °C, and the elongation is 34%. While increasing the temperature to 1000°C resulted in a lower yield strength of 1000 MPa and an ultimate tensile strength of 1441 MPa with a slightly higher elongation of 38%. In order to study the impact of Nb content on the structure, phases, and mechanical properties, the 950°C aging condition will be used throughout this work. Even though recrystallization may start to happen before 950°C at lower Nb compositions, the difference is incredibly small. In order to study various Nb compositions, the study kept the temperature at 950°C.

Different Niobium Contents in Samples Analysis at a Constant Temperature

Microstructure of HEA0, HEA1, and HEA3 at 950°C.

Fig. 19 depicts the microstructures of the samples aged at 950°C for 1 hour with Nb contents of 0% (HEA0), 1% (HEA1), and 3% (HEA3). All samples exhibit recrystallized grains with twin structures, as can be seen. This demonstrated that 950°C is sufficient to cause the structure in these HEAs to recrystallize. The results of calculating the grain sizes for the samples HEA0, HEA1, and HEA3 are 77 m, 12 m, and 40 m, respectively. The HEA5 sample's grain size was 45 m as well. When the specimen was kept at 1200 °C with a 0.045% Nb addition, the average grain size decreased from 242 μm to 172 μm, demonstrating that the presence of Nb successfully refines grains at the investigated temperatures. Wu et al. (2018) conducted another study to examine the impact of Nb and V content on steel alloys. This is also evident in the microstructure findings of this thesis, where the grain size decreases as the Nb content rises.

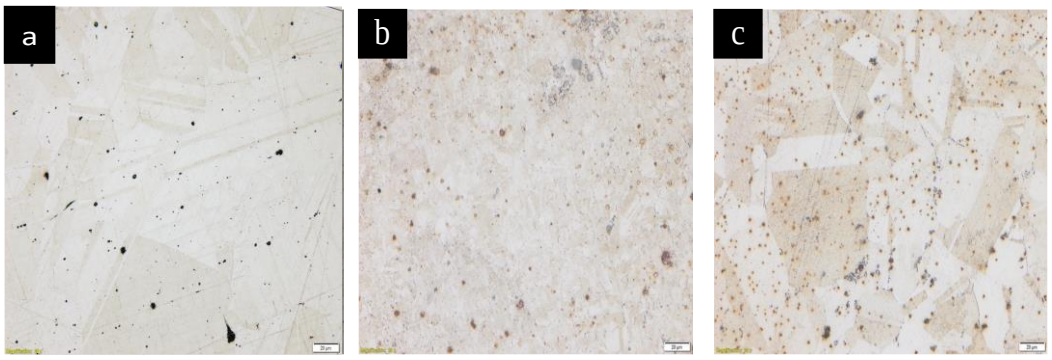

Figure 21: Microstructure ananylsis by opyical microscopy for alloy $Ni_{0.55}CoCrAlNb_x$ aged samples at 950°C : (a) HEA0 sample, (b) HEA1 sample, and (c) HEA3 sample.

X-Ray diffraction of HEA0, HEA1, and HEA3 at 950°C.

The main phase is FCC crystalline structure which is depicted in the five peaks for the HEA0, HEA1, and HEA3 samples seen in Figure 20. There are minor peaks seen in aged at 950 ºC sample. These peaks could be the second phase that showed up after the aging. This confirms that recrystallization is initiated. The diffraction peaks gradually rise as Nb concentration rises, indicating that the lattice parameters of the solid solution phases of FCC and B2 grew. The findings of Jiang et al investigation are supported by this outcome (2020). They saw a significant lattice distortion and higher FCC and B2 lattice parameters when they raised the Nb concentration in their cast. This is brought on by the element Nb's high atomic radius melting into the phases.

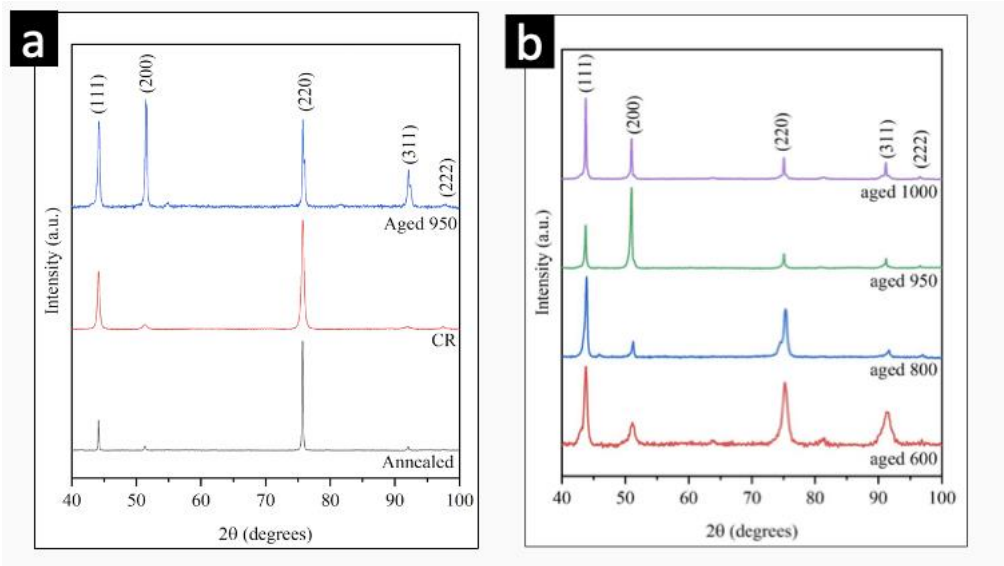

Figure 22: (a) XRD patterns of the HEAs with different Nb contents aged at 950 ºC for 1 hr. (b) XRD patterns HEA5 at different aging temperatures

Mechanical Properties of HEA0, HEA1, and HEA3 at 950°C

Microhardness of HEA0, HEA1, and HEA3 at 950°C.

The hardness was calculated before aging the samples. The annealing hardness results for HEA0, HEA1, and HEA3 samples are shown in Figure 21. After annealing, the samples' thicknesses were reduced by 90%, 85%, and 62% of the HEA0, HEA1, and HEA3 samples during cold rolling. The hardest sample, with a value of 3.8 GPa, was HEA3. This may be explained by the fact that when we reduce the Nb %, the hardness will also decrease relative to HEA5. Similar effects of Nb inclusion on the cast alloy AlCoCrFeNi2.1Nbx were observed in Jiang et al. work .'s from 2022 with regard to hardness. These alloys' Vickers hardness increased noticeably from 6.26 x 10-7 GPa to 1.998 x 10-6 GPa when their Nb concentration rose from 0 to 0.05. This was explained by the second-phase precipitation hardening and the FCC solid solution strengthening that could play a significant role in this hardening mechanism.

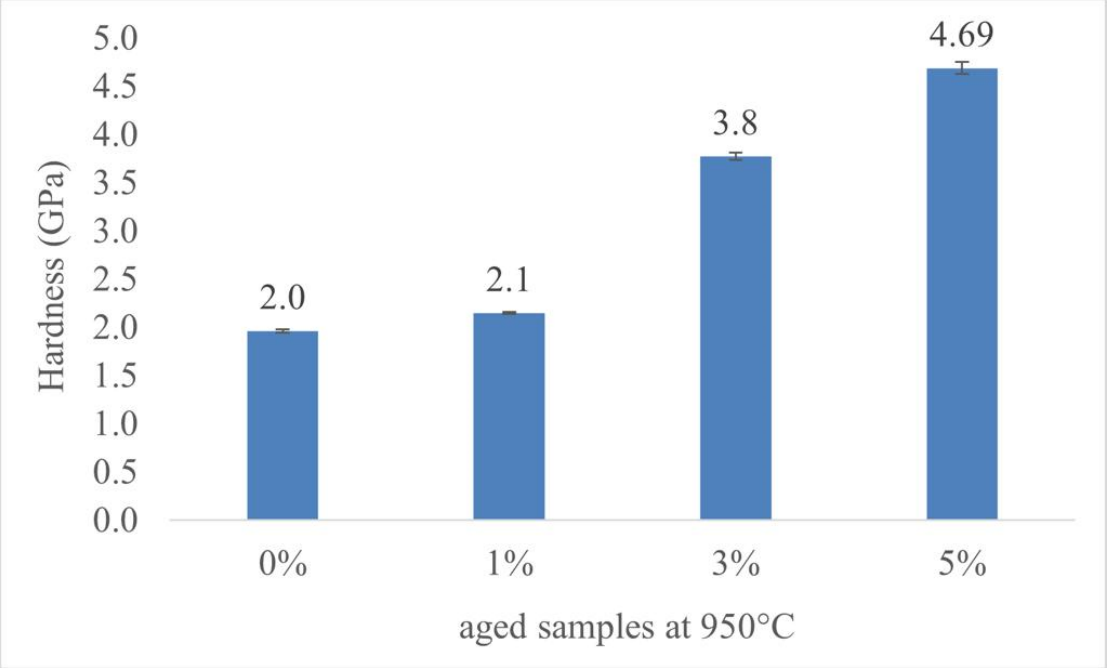

Figure 23: A bar graph comparison of microhardness and the different composition of HEA0, HEA1, HEA3, and HEA5 aged 950 ºC.

Tensile of HEA0, HEA1, and HEA3 at 950°C.

Figure 22 shows the tensile stress of aged at 950 °C for the three samples. As the content of Nb is increased from 0% to 3% in the study, the graph displays that the yield strength increases as well by 161 MPa, 298 MPa, and 777 MPa, respectively. However, the modulus results don't show any pattern to reflect on; the highest value was the HEA1 sample which is 272 GPa. Both the HEA0 sample elasticity and the HEA3 material stiffness are fairly similar at 170 GPa and 169 GPa, respectively. When compared to the HEA5 sample's data mentioned above, the elastic modulus is still the greatest at 1050 MPa. As the Nb content increased, the elongation results dropped. The elongation percentages for HEA0, HEA1, and HEA3 Nb samples are 88%, 61%, and 31%, respectively. Nevertheless, Figure 23 shows the stress-strain engineering graph for all samples. The HEA5 Nb sample had an elongation of 34%. This confirms that the most effective ductility and yield strength combination would be in the HEA5 sample. Many scholars suggest that the improved ductility is caused by the strengthening of the grain boundary, the strengthening of the dislocation, the strengthening of the solid solution, and the strengthening of the precipitation. Finally, the tensile strength was also calculated as shown in Table 3, for HEA0, HEA1 and HEA3 samples as follows: 535 MPa, 707 MPa, and 1193 MPa, respectively. Whereas the HEA5 sample had the highest tensile strength, 1534 MPa, it can withstand higher stress without cracking.

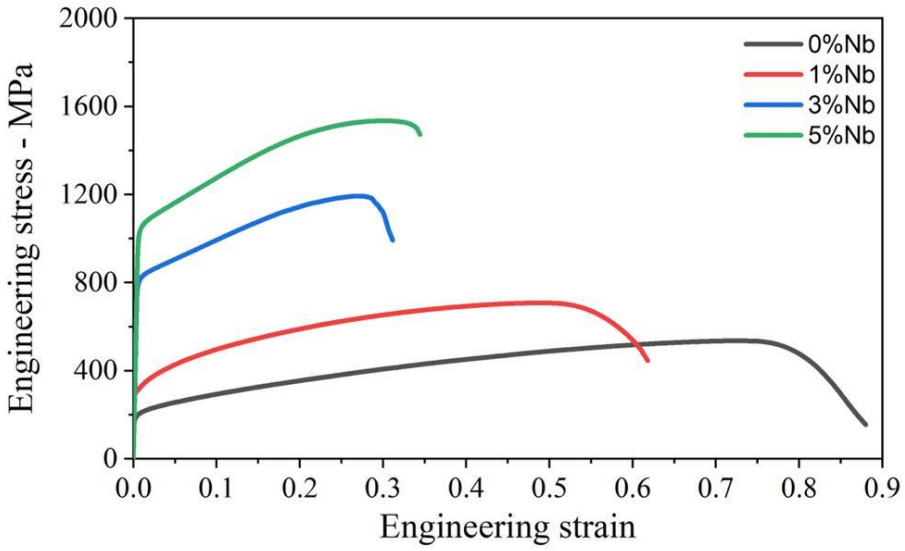

Figure 22: Stress-strain engineering graph for all samples aged at 950 °C

The work by Jiang et al. (2022) demonstrated the superiority of enhancing the mechanical characteristics of the AlCoCrFeNi2.1 alloy by adding Nb content. In their study, the yield strength increased from 626 MPa to 1998 MPa as the Nb content grew from 0 to 0.05. This significant difference is comparable to increasing the NiCoCrAlNbx(x=0, x=1, x=3, and x=5) alloy's Nb content from 0 to 0.05. There is an increase in yield strength from 169 MPa to 1050 MPa. The FCC solid solution, which has tiny peaks visible in the XRD, is responsible for this occurrence. Strength and plasticity are best balanced by the phase combination.

Table 3: Mechanical properties results of $NiCoCrAlNb_x$ (x= 0, 0.01,0.03, and 0.05) Nb samples aged at 950 °C.

	σy (MPa)	σ (MPa)	δ %
HEA0	161	535	88
HEA1	298	707	61
HEA3	777	1193	31
HEA5	1050	1534	34

Fracture surface analysis of HEA0, HEA1, and HEA3 at 950°C:

The SEM analysis was done for the 1% sample and 3% sample since they acquired higher hardness and yield strength. The voids in Figure 23a-b are seen as less than what Figure 20 displays. This excessive number of voids in Figure 23b reflects the elongation attained by a higher content of Nb. Consequently, a relationship can be made between the number of voids and the improvement of elongation. It is directly proportional; as the voids number increased due to higher Nb content, the elongation of the material is further improved. Contrary to it, the HEA5 sample image in Figure 23, at 950 °C had higher voids or tears than the 1% and 3% sample due to its elongation being equal to 34%. According to Lu et al. (2017) and Jiang et al. (2021), both studies explain that the voids or fractures displayed in the SEM images ductility tear edge and elongated groove microstructure. These tears are very similar to a high entropy alloy Lu et al. have worked on called - $AlCoCrFeNi_{2.1}$.

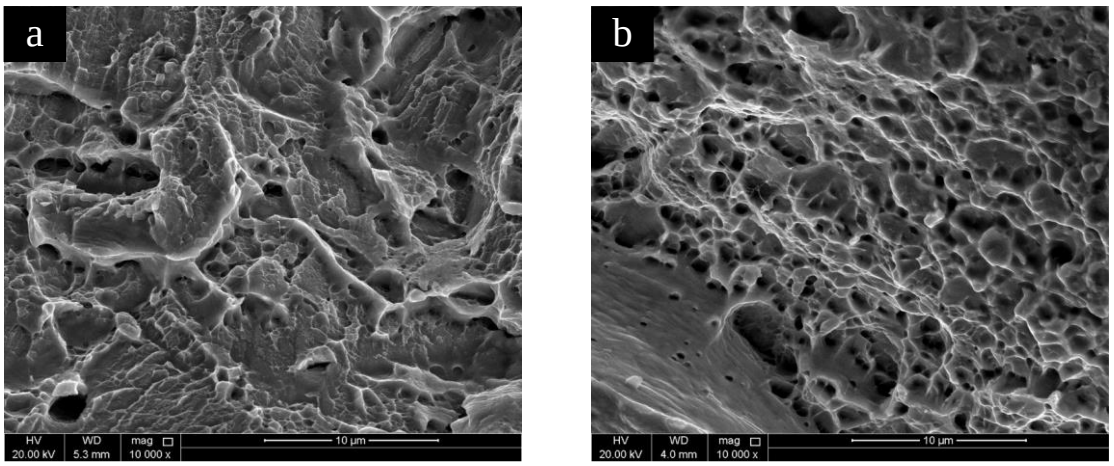

Figure 23: High magnification SEM BSE images of as-cast NiCoCrAlNbx HEAs alloys aged at 950°C: (a) HEA1 sample and (b)HEA3 sample.

Chapter 5: Conclusion

This research sought to identify a stable composition of a high entropy alloy with an optimal microstructure and mechanical properties based on the required application of the high entropy alloy. Arc melting under an argon environment was used to successfully prepare the high entropy NiCoCrAlNbx (x=0, x=1, x=3, and x=5) alloy. HEA5 sample was composed and treated at different temperatures. This attempt concluded that the HEA5 samples are best treated under a temperature of 950 °C, having the optimum ductility and grain size compared to the other temperatures. Next, the study proceeded for the HEAs samples: HEA0, HEA1, and HEA3 by only analyzing the characteristics under the aging temperature of 950 °C. The remarks of the analysis were that with the Nb content increase, grain size is flatulated. In HEA0, the grain size was 77 μm which is much greater than the other compositions due to the absence of Nb. However, in the slight presence of Nb, HEA1, the grain size dropped to 12 μm. As the Nb content increased to HEA3 and HEA5, the grain size grew further to 40 μm and 45 μm, respectively. In the XRD analysis, the main phase is FCC-HEAs. In the samples aged at 950 ºC minor peaks were depicted, showing a second phase confirming recrystallization being initiated. Moreover, by increasing the Nb from 0% to 5%, the stability of the phases showed single-phase FCC-HEAs. The hardness of the samples increased as the Nb content increased. Furthermore, as hardness increases the material risks being more brittle. The yield strength, fracture strength, and plastic strain rise from around 161 MPa to 1050 MPa by increasing the Nb from 0% to 5%. Because of the strengthening and fine grain strengthening of the Nb atom, the yield strength has increased. The four samples' elongation decreased as Nb concentration rose from 0% to 5%. This can be explained that the material became more brittle as hardness increased which confirms the facts stated by Charles and Das (2017) about niobium. In

conclusion, the ideal composition percentage for industrial applications is the HEA5 aging at a temperature of 950 °C.

References

Abu-Odeh, A., Galvan, E., Kirk, T., Mao, H., Chen, Q., Mason, P., Malak, R., & Arróyave, R. (2018). Efficient exploration of the high entropy alloy composition-phase space. *Acta Materialia*, *152*, 41–57. https://doi.org/10.1016/j.actamat.2018.04.012

Abuzaid, W., & Sehitoglu, H. (2017). Critical resolved shear stress for slip and twin nucleation in single crystalline FeNiCoCrMn high entropy alloy. *Materials Characterization*, *129*, 288–299. https://doi.org/10.1016/j.matchar.2017.05.014

Borkar, T., Chaudhary, V., Gwalani, B., Choudhuri, D., Mikler, C. V., Soni, V., Alam, T., V. Ramanujan, R., & Banerjee, R. (2017). A combinatorial approach for assessing the magnetic properties of high entropy alloys: Role of CR in alco *x* cr1-*x* feni. *Advanced Engineering Materials*, *19*(8), 1700048. https://doi.org/10.1002/adem.201700048

Borkar, T., Gwalani, B., Choudhuri, D., Mikler, C. V., Yannetta, C. J., Chen, X., Ramanujan, R. V., Styles, M. J., Gibson, M. A., & Banerjee, R. (2016). A combinatorial assessment of ALXCRCUFENI2 (0 < x < 1.5) complex concentrated alloys: Microstructure, microhardness, and magnetic properties. *Acta Materialia*, *116*, 63–76. https://doi.org/10.1016/j.actamat.2016.06.025

Bracq, G., Laurent-Brocq, M., Perrière, L., Pirès, R., Joubert, J.-M., & Guillot, I. (2017). The FCC solid solution stability in the Co-Cr-Fe-Mn-Ni multi-component system. *Acta Materialia*, *128*, 327–336. https://doi.org/10.1016/j.actamat.2017.02.017

Butt, M. Z., & Feltham, P. (1980). Solid-solution hardening of dilute alloys. *August 16*, 729–732. https://doi.org/10.1515/9783112501900-054

Cabibbo, M., Průša, F., Šenková, A., Školáková, A., Kučera, V., & Veselka, Z. (2020). Compression stress strengthening modelling of a ultrafine-grained equiatomic SPS cocrfeninb high-entropy alloy. *Proceedings of the Institution of Mechanical Engineers, Part C: Journal of Mechanical Engineering Science*, *235*(8), 1432–1442. https://doi.org/10.1177/0954406220943245

Cai, Z., Jiang, F., Wei, N., Mi, L., Zhang, C., Liu, X., Si, F., & Wu, T. (2022). Effect of annealing temperatures on phase stability, mechanical properties, and high-temperature steam corrosion resistance of (Feni)67cr15mn10al5ti3 alloy. *Metals, 12*(9), 1467. https://doi.org/10.3390/met12091467

Cantor, B., Chang, I. T. H., Knight, P., & Vincent, A. J. B. (2004). Microstructural development in equiatomic multicomponent alloys. *Materials Science and Engineering: A*, *375-377*, 213–218. https://doi.org/10.1016/j.msea.2003.10.257

Chanda, B., & Das, J. (2017). Composition dependence on the evolution of Nanoeutectic in CoCrFeNiNbx ($0.45 \leq x \leq 0.65$) high entropy alloys. *Advanced Engineering Materials*, *20*(4), 1700908. https://doi.org/10.1002/adem.201700908

Chen, X., Xie, W., Zhu, J., Wang, Z., Wang, Y., Ma, Y., Yang, M., Jiang, W., Yu, H., Wu, Y., & Hui, X. (2021). Influences of Ti additions on the microstructure and tensile properties of alcocrfeni2.1 eutectic high entropy alloy. *Intermetallics*, *128*, 107024. https://doi.org/10.1016/j.intermet.2020.107024

Cieslak, J., Tobola, J., Berent, K., & Marciszko, M. (2018). Phase composition of

alxfenicrco high entropy alloys prepared by sintering and Arc-Melting Methods. *Journal of Alloys and Compounds*, *740*, 264–272. https://doi.org/10.1016/j.jallcom.2017.12.333

Collins, P. C., Banerjee, R., Banerjee, S., & Fraser, H. L. (2003). Laser deposition of compositionally graded titanium–vanadium and titanium–molybdenum alloys. *Materials Science and Engineering: A*, *352*(1-2), 118–128. https://doi.org/10.1016/s0921-5093(02)00909-7

Couzinié, J. P., Dirras, G., Perrière, L., Chauveau, T., Leroy, E., Champion, Y., & Guillot, I. (2014). Microstructure of a near-equimolar refractory high-entropy alloy. *Materials Letters*, *126*, 285–287. https://doi.org/10.1016/j.matlet.2014.04.062

Coyne-Grell, A., Blaizot, J., Rahimi, S., Violatos, I., Nouveau, S., Dumont, C., Nicolaÿ, A., & Bozzolo, N. (2022). Recrystallization mechanisms and associated microstructure evolution during billet conversion of a gamma-gamma′ nickel based superalloy. Journal of Alloys and Compounds, *916*, 165465. https://doi.org/10.1016/j.jallcom.2022.165465

Detrois, M., Antonov, S., & Tin, S. (2019). Phase stability and thermodynamic database validation in a set of non-equiatomic al-co-cr-fe-nb-ni high-entropy alloys. *Intermetallics*, *104*, 103–112. https://doi.org/10.1016/j.intermet.2018.11.002

Dirras, G., Gubicza, J., Heczel, A., Lilensten, L., Couzinié, J.-P., Perrière, L., Guillot, I., & Hocini, A. (2015). Microstructural investigation of plastically deformed Ti20zr20hf20nb20ta20 high entropy alloy by X-ray diffraction and transmission electron microscopy. *Materials Characterization*, *108*, 1–7. https://doi.org/10.1016/j.matchar.2015.08.007

Dirras, G., Lilensten, L., Djemia, P., Laurent-Brocq, M., Tingaud, D., Couzinié, J.-P., Perrière, L., Chauveau, T., & Guillot, I. (2016). Elastic and plastic properties of AS-cast equimolar tihfzrtanb high-entropy alloy. *Materials Science and Engineering: A*, *654*, 30–38. https://doi.org/10.1016/j.msea.2015.12.017

Dobbelstein, H., Gurevich, E. L., George, E. P., Ostendorf, A., & Laplanche, G. (2019). Laser metal deposition of compositionally graded TIZRNBTA refractory high-entropy alloys using elemental powder blends. *Additive Manufacturing*, *25*, 252–262. https://doi.org/10.1016/j.addma.2018.10.042

Dong, Y., & Lu, Y. (2019). Microstructure and Mechanical Properties of CoCrFeNi2Al1−x Wx High Entropy Alloys. *Arabian Journal for Science and Engineering*, *44*(2), 803-808. doi:10.1007/s13369-018-3297-9

Gao, M. C., Zhang, C., Gao, P., Zhang, F., Ouyang, L. Z., Widom, M., & Hawk, J. A. (2017). Thermodynamics of concentrated solid solution alloys. *Current Opinion in Solid State and Materials Science*, *21*(5), 238–251. https://doi.org/10.1016/j.cossms.2017.08.001

Gludovatz, B., Hohenwarter, A., Catoor, D., Chang, E. H., George, E. P., & Ritchie, R. O. (2014). Cheminform abstract: A fracture-resistant high-entropy alloy for cryogenic applications. *ChemInform*, *45*(47). https://doi.org/10.1002/chin.201447007

Gorsse, S., & Tancret, F. (2018). Current and emerging practices of Calphad toward the development of high entropy alloys and complex concentrated alloys. *Journal of Materials Research*, *33*(19), 2899–2923. https://doi.org/10.1557/jmr.2018.152

Gu, J., Ni, S., Liu, Y., & Song, M. (2019). Regulating the strength and ductility of a cold rolled FeCrCoMnNi high-entropy alloy via annealing treatment. *Materials Science and Engineering: A, 755*, 289–294. https://doi.org/10.1016/j.msea.2019.04.025

GUO, S., & LIU, C. T. (2011). Phase stability in high entropy alloys: Formation of solid-solution phase or amorphous phase. *Progress in Natural Science: Materials International, 21*(6), 433–446. https://doi.org/10.1016/s1002-0071(12)60080-x

Haase, C., & Barrales-Mora, L. A. (2018). Influence of deformation and annealing twinning on the microstructure and texture evolution of face-centered cubic high-entropy alloys. *Acta Materialia, 150*, 88–103. https://doi.org/10.1016/j.actamat.2018.02.048

Haasen, P. (1958). Plastic deformation of nickel single crystals at low temperatures. *Philosophical Magazine, 3*(28), 384–418. https://doi.org/10.1080/14786435808236826

He, F., Wang, Z., Wu, Q., Chen, D., Yang, T., Li, J., Wang, J., Liu, C. T., & Kai, J.-jung. (2018). Tuning the defects in face centered cubic high entropy alloy via temperature-dependent stacking fault energy. *Scripta Materialia, 155*, 134–138. https://doi.org/10.1016/j.scriptamat.2018.06.002

He, J. Y., Wang, H., Huang, H. L., Xu, X. D., Chen, M. W., Wu, Y., Liu, X. J., Nieh, T. G., An, K., & Lu, Z. P. (2016). A precipitation-hardened high-entropy alloy with outstanding tensile properties. *Acta Materialia, 102*, 187–196. https://doi.org/10.1016/j.actamat.2015.08.076

Hou, J., Shi, X., Qiao, J., Zhang, Y., Liaw, P. K., & Wu, Y. (2019). Ultrafine-grained dual phase al0.45cocrfeni high-entropy alloys. *Materials & Design*, *180*, 107910. https://doi.org/10.1016/j.matdes.2019.107910

Hou, L., Hui, J., Yao, Y., Chen, J., & Liu, J. (2019). Effects of boron content on microstructure and mechanical properties of alfeconibx high entropy alloy prepared by vacuum arc melting. *Vacuum*, *164*, 212–218. https://doi.org/10.1016/j.vacuum.2019.03.019

Huang, H., Wu, Y., He, J., Wang, H., Liu, X., An, K., Wu, W., & Lu, Z. (2017). Phase-transformation ductilization of brittle high-entropy alloys via Metastability Engineering. *Advanced Materials*, *29*(30), 1701678. https://doi.org/10.1002/adma.201701678

Huang, P.-K., Yeh, J.-W., Shun, T.-T., & Chen, S.-K. (2004). Multi-principal-element alloys with improved oxidation and wear resistance for thermal spray coating. *Advanced Engineering Materials*, *6*(12), 74–78. https://doi.org/10.1002/adem.200300507

Huang, S., Li, W., Lu, S., Tian, F., Shen, J., Holmström, E., & Vitos, L. (2015). Temperature dependent stacking fault energy of FeCrCoNiMn high entropy alloy. *Scripta Materialia, 108*, 44–47. https://doi.org/10.1016/j.scriptamat.2015.05.041

Jiang, H., Li, L., Ni, Z., Qiao, D., Zhang, Q., & Sui, H. (2022). Effect of NB on microstructure and properties of alcocrfeni2.1 high entropy alloy. *Materials Chemistry and Physics, 290*, 126631. https://doi.org/10.1016/j.matchemphys.2022.126631

Jiang, H., Qiao, D., Jiao, W., Han, K., Yiping, L., & Liaw, P. K. (2021). Tensile

deformation behavior and mechanical properties of a bulk cast Al0.9COFENI2 eutectic high-entropy alloy. *Journal of Materials Science & Technology*, *61*, 119–124. https://doi.org/10.1016/j.jmst.2020.05.053

Juan, C.-C., Tsai, M.-H., Tsai, C.-W., Lin, C.-M., Wang, W.-R., Yang, C.-C., Chen, S.-K., Lin, S.-J., & Yeh, J.-W. (2015). Enhanced mechanical properties of HFMOTATIZR and HFMONBTATIZR refractory high-entropy alloys. *Intermetallics*, *62*, 76–83. https://doi.org/10.1016/j.intermet.2015.03.013

Khan, T. Z., Kirk, T., Vazquez, G., Singh, P., Smirnov, A. V., Johnson, D. D., Youssef, K., & Arróyave, R. (2022). Towards stacking fault energy engineering in FCC High Entropy Alloys. *Acta Materialia*, *224*, 117472. https://doi.org/10.1016/j.actamat.2021.117472

Kireeva, I. V., Chumlyakov, Y. I., Pobedennaya, Z. V., Kuksgausen, I. V., & Karaman, I. (2017). Orientation dependence of twinning in single crystalline cocrfemnni high-entropy alloy. *Materials Science and Engineering: A*, *705*, 176–181. https://doi.org/10.1016/j.msea.2017.08.065

Kirk, T., Vela, B., Mehalic, S., Youssef, K., & Arróyave, R. (2022). Entropy-driven melting point depression in FCC HEAS. *Scripta Materialia*, *208*, 114336. https://doi.org/10.1016/j.scriptamat.2021.114336

Knoll, H., Ocylok, S., Weisheit, A., Springer, H., Jägle, E., & Raabe, D. (2016). Combinatorial alloy design by laser additive manufacturing. *Steel Research International*, *88*(8), 1600416. https://doi.org/10.1002/srin.201600416

Komarasamy, M., Alagarsamy, K., & Mishra, R. S. (2017). Serration behavior and negative strain rate sensitivity of al0.1cocrfeni high entropy alloy. *Intermetallics*, *84*, 20–24. https://doi.org/10.1016/j.intermet.2016.12.016

Lilensten, L., Couzinié, J. P., Perrière, L., Bourgon, J., Emery, N., & Guillot, I. (2014). New structure in refractory high-entropy alloys. *Materials Letters*, *132*, 123–125. https://doi.org/10.1016/j.matlet.2014.06.064

Lima Filho, V. X., Barros, I. F., & Abreu, H. F. (2016). Influence of solution annealing on microstructure and mechanical properties of maraging 300 steel. *Materials Research*, *20*(1), 10–14. https://doi.org/10.1590/1980-5373-mr-2016-0257

Lin, C.-M., Juan, C.-C., Chang, C.-H., Tsai, C.-W., & Yeh, J.-W. (2015). Effect of al addition on mechanical properties and microstructure of refractory alxhfnbtatizr alloys. *Journal of Alloys and Compounds*, *624*, 100–107. https://doi.org/10.1016/j.jallcom.2014.11.064

Liu, S. F., Wu, Y., Wang, H. T., He, J. Y., Liu, J. B., Chen, C. X., Liu, X. J., Wang, H., & Lu, Z. P. (2018). Stacking fault energy of face-centered-cubic high entropy alloys. *Intermetallics*, *93*, 269–273. https://doi.org/10.1016/j.intermet.2017.10.004

Liu, W. H., Wu, Y., He, J. Y., Nieh, T. G., & Lu, Z. P. (2013). Grain growth and the hall–petch relationship in a high-entropy fecrnicomn alloy. *Scripta Materialia*, *68*(7), 526–529. https://doi.org/10.1016/j.scriptamat.2012.12.002

Lu, W., Luo, X., Yang, Y., Yan, K., Huang, B., & Li, P. (2020). Nano-precipitates strengthened non-equiatomic medium-entropy alloy with outstanding tensile

properties. *Materials Science and Engineering: A*, *780*, 139218. https://doi.org/10.1016/j.msea.2020.139218

Lu, Y., Gao, X., Jiang, L., Chen, Z., Wang, T., Jie, J., Kang, H., Zhang, Y., Guo, S., Ruan, H., Zhao, Y., Cao, Z., & Li, T. (2017). Directly cast bulk eutectic and near-eutectic high entropy alloys with balanced strength and ductility in a wide temperature range. *Acta Materialia*, *124*, 143–150. https://doi.org/10.1016/j.actamat.2016.11.016

Luo, H., Li, Z., & Raabe, D. (2017). Hydrogen enhances strength and ductility of an equiatomic high-entropy alloy. *Scientific Reports*, *7*(1). https://doi.org/10.1038/s41598-017-10774-4

Luo, H., Lu, W., Fang, X., Ponge, D., Li, Z., & Raabe, D. (2018). Beating hydrogen with its own weapon: Nano-twin gradients enhance embrittlement resistance of a high-entropy alloy. *Materials Today*, *21*(10), 1003–1009. https://doi.org/10.1016/j.mattod.2018.07.015

Ma, D., Yao, M., Pradeep, K. G., Tasan, C. C., Springer, H., & Raabe, D. (2015). Phase stability of non-equiatomic cocrfemnni high entropy alloys. *Acta Materialia*, *98*, 288–296. https://doi.org/10.1016/j.actamat.2015.07.030

Masemola, K., Popoola, P., & Malatji, N. (2020). The effect of annealing temperature on the microstructure, mechanical and electrochemical properties of Arc-Melted alcrfemnni equi-atomic high entropy alloy. *Journal of Materials Research and Technology*, *9*(3), 5241–5251. https://doi.org/10.1016/j.jmrt.2020.03.050

Miracle, D. B., & Senkov, O. N. (2017). A critical review of high entropy alloys and related concepts. *Acta Materialia*, *122*, 448–511.

https://doi.org/10.1016/j.actamat.2016.08.081

Nene, S. S., Liu, K., Frank, M., Mishra, R. S., Brennan, R. E., Cho, K. C., Li, Z., & Raabe, D. (2017). Enhanced strength and ductility in a friction stir processing engineered dual phase high entropy alloy. *Scientific Reports*, *7*(1). https://doi.org/10.1038/s41598-017-16509-9

Niu, Z., Xie, Y., Axinte, E., Xu, J., & Wang, Y. (2020). Development and characterization of novel ni-rich high-entropy alloys. *Journal of Alloys and Compounds*, *846*, 156342. https://doi.org/10.1016/j.jallcom.2020.156342

Nong, Z.-S., Wang, H.-Y., Wang, D.-P., & Zhu, J.-C. (2020). Investigation on structural stability of AS-cast al0.5crcufemnti high entropy alloy. *Vacuum*, *182*, 109686. https://doi.org/10.1016/j.vacuum.2020.109686

Okamoto, N. L., Yuge, K., Tanaka, K., Inui, H., & George, E. P. (2016). Atomic displacement in the CRMNFECONI high-entropy alloy – a scaling factor to predict solid solution strengthening. *AIP Advances*, *6*(12), 125008. https://doi.org/10.1063/1.4971371

Otto, F., Dlouhý, A., Pradeep, K. G., Kuběnová, M., Raabe, D., Eggeler, G., & George, E. P. (2016). Decomposition of the single-phase high-entropy alloy CRMNFECONI after prolonged anneals at intermediate temperatures. *Acta Materialia*, *112*, 40–52. https://doi.org/10.1016/j.actamat.2016.04.005

Otto, F., Yang, Y., Bei, H., & George, E. P. (2013). Relative effects of enthalpy and entropy on the phase stability of equiatomic high-entropy alloys. *Acta Materialia*, *61*(7), 2628–2638. https://doi.org/10.1016/j.actamat.2013.01.042

Park, T., & Kim, J. H. (2020). Tensile properties and microstructure evolution during two-stage tensile testing of cocrfemnni high-entropy alloy. *Journal of Materials Research and Technology*, *9*(4), 7551–7557. https://doi.org/10.1016/j.jmrt.2020.05.069

Pickering, E. J., & Jones, N. G. (2016). High-entropy alloys: A critical assessment of their founding principles and future prospects. *International Materials Reviews*, *61*(3), 183–202. https://doi.org/10.1080/09506608.2016.1180020

Pickering, E. J., Muñoz-Moreno, R., Stone, H. J., & Jones, N. G. (2016). Precipitation in the equiatomic high-entropy alloy CrMnFeCoNi. *Scripta Materialia*, *113*, 106–109. https://doi.org/10.1016/j.scriptamat.2015.10.025

Pradeep, K. G., Tasan, C. C., Yao, M. J., Deng, Y., Springer, H., & Raabe, D. (2015). Non-equiatomic high entropy alloys: Approach towards rapid alloy screening and property-oriented design. *Materials Science and Engineering: A*, *648*, 183–192. https://doi.org/10.1016/j.msea.2015.09.010

Průša, F., Cabibbo, M., Šenková, A., Kučera, V., Veselka, Z., Školáková, A., Vojtěch, D., Cibulková, J., & Čapek, J. (2020). High-strength ultrafine-grained cocrfeninb high-entropy alloy prepared by mechanical alloying: Properties and strengthening mechanism. *Journal of Alloys and Compounds*, *835*, 155308. https://doi.org/10.1016/j.jallcom.2020.155308

Rar, A., Frafjord, J. J., Fowlkes, J. D., Specht, E. D., Rack, P. D., Santella, M. L., Bei, H., George, E. P., & Pharr, G. M. (2004). PVD synthesis and high-throughput property characterization of Ni–Fe–Cr Alloy Libraries. *Measurement Science and Technology*, *16*(1), 46–53. https://doi.org/10.1088/0957-0233/16/1/007

Senkov, O. N., Wilks, G. B., Miracle, D. B., Chuang, C. P., & Liaw, P. K. (2010). Refractory high-entropy alloys. *Intermetallics*, *18*(9), 1758–1765. https://doi.org/10.1016/j.intermet.2010.05.014

Senkov, O. N., Wilks, G. B., Scott, J. M., & Miracle, D. B. (2011). Mechanical properties of NB25MO25TA25W25 and V20NB20MO20TA20W20 refractory high entropy alloys. *Intermetallics*, *19*(5), 698–706. https://doi.org/10.1016/j.intermet.2011.01.004

Seol, J. B., Bae, J. W., Li, Z., Chan Han, J., Kim, J. G., Raabe, D., & Kim, H. S. (2018). Boron doped ultrastrong and ductile high-entropy alloys. *Acta Materialia*, *151*, 366–376. https://doi.org/10.1016/j.actamat.2018.04.004

Shabani, A., Toroghinejad, M. R., Shafyei, A., & Logé, R. E. (2019). Evaluation of the mechanical properties of the heat treated fecrcumnni high entropy alloy. *Materials Chemistry and Physics*, *221*, 68–77. https://doi.org/10.1016/j.matchemphys.2018.09.033

Shang, C., Axinte, E., Sun, J., Li, X., Li, P., Du, J., Qiao, P., & Wang, Y. (2017). Cocrfeni(W1−xMox) high-entropy alloy coatings with excellent mechanical properties and corrosion resistance prepared by mechanical alloying and Hot Pressing Sintering. *Materials & Design*, *117*, 193–202. https://doi.org/10.1016/j.matdes.2016.12.076

Shao, Y., Ma, H., & Wang, Y. (2020). Effect of mo addition on the microstructure and mechanical properties of cocufeni high entropy alloy. *Metals*, *10*(8), 1017. https://doi.org/10.3390/met10081017

Sharma, A. (2020). High-entropy alloys for micro- and Nanojoining applications.

Engineering Steels and High Entropy-Alloys. https://doi.org/10.5772/intechopen.91166

Sheikh, S., Shafeie, S., Hu, Q., Ahlström, J., Persson, C., Veselý, J., Zýka, J., Klement, U., & Guo, S. (2016). Alloy design for intrinsically ductile refractory high-entropy alloys. *Journal of Applied Physics*, *120*(16), 164902. https://doi.org/10.1063/1.4966659

Slone, C. E., Miao, J., George, E. P., & Mills, M. J. (2019). Achieving ultra-high strength and ductility in equiatomic CrCoNi with partially recrystallized microstructures. *Acta Materialia*, *165*, 496–507. https://doi.org/10.1016/j.actamat.2018.12.015

Song, H., Tian, F., & Wang, D. (2016). Thermodynamic properties of refractory high entropy alloys. *Journal of Alloys and Compounds*, *682*, 773–777. https://doi.org/10.1016/j.jallcom.2016.04.320

Specht, E. D., Rar, A., Pharr, G. M., George, E. P., Zschack, P., Hong, H., & Ilavsky, J. (2003). Rapid structural and chemical characterization of ternary phase diagrams using synchrotron radiation. *Journal of Materials Research*, *18*(10), 2522–2527. https://doi.org/10.1557/jmr.2003.0351

Springer, H., & Raabe, D. (2012). Rapid alloy prototyping: Compositional and thermo-mechanical high throughput bulk combinatorial design of structural materials based on the example of 30Mn–1.2C–xal triplex steels. *Acta Materialia*, *60*(12), 4950–4959. https://doi.org/10.1016/j.actamat.2012.05.017

Steinmetz, D. R., Jäpel, T., Wietbrock, B., Eisenlohr, P., Gutierrez-Urrutia, I., Saeed–Akbari, A., Hickel, T., Roters, F., & Raabe, D. (2013). Revealing the strain-hardening behavior of twinning-induced plasticity steels: Theory, simulations, experiments. *Acta Materialia*, *61*(2), 494–510.

https://doi.org/10.1016/j.actamat.2012.09.064

Tasan, C. C., Deng, Y., Pradeep, K. G., Yao, M. J., Springer, H., & Raabe, D. (2014). Composition dependence of phase stability, deformation mechanisms, and mechanical properties of the COCRFEMNNI high-entropy alloy system. *JOM*, *66*(10), 1993–2001. https://doi.org/10.1007/s11837-014-1133-6

Tsai, M.-H., & Yeh, J.-W. (2014). High-entropy alloys: A critical review. *Materials Research Letters*, *2*(3), 107–123. https://doi.org/10.1080/21663831.2014.912690

Varvenne, C., Leyson, G. P. M., Ghazisaeidi, M., & Curtin, W. A. (2017). Solute strengthening in random alloys. *Acta Materialia*, *124*, 660–683. https://doi.org/10.1016/j.actamat.2016.09.046

Varvenne, C., Luque, A., & Curtin, W. A. (2016). Theory of strengthening in FCC high entropy alloys. *Acta Materialia*, *118*, 164–176. https://doi.org/10.1016/j.actamat.2016.07.040

Vazquez, G., Singh, P., Sauceda, D., Couperthwaite, R., Britt, N., Youssef, K., Johnson, D. D., & Arróyave, R. (2022). Efficient machine-learning model for fast assessment of elastic properties of high-entropy alloys. *Acta Materialia*, *232*, 117924. https://doi.org/10.1016/j.actamat.2022.117924

Wang, M., Li, Z., & Raabe, D. (2018). In-situ sem observation of phase transformation and twinning mechanisms in an interstitial high-entropy alloy. *Acta Materialia*, *147*, 236–246. https://doi.org/10.1016/j.actamat.2018.01.036

Wani, I. S., Bhattacharjee, T., Sheikh, S., Bhattacharjee, P. P., Guo, S., & Tsuji, N. (2016). Tailoring nanostructures and mechanical properties of alcocrfeni2.1 eutectic

high entropy alloy using thermo-mechanical processing. *Materials Science and Engineering: A, 675*, 99–109. https://doi.org/10.1016/j.msea.2016.08.048

Wani, I. S., Bhattacharjee, T., Sheikh, S., Bhattacharjee, P. P., Guo, S., & Tsuji, N. (2016). Tailoring nanostructures and mechanical properties of alcocrfeni2.1 eutectic high entropy alloy using thermo-mechanical processing. *Materials Science and Engineering: A, 675*, 99-109. https://doi.org/10.1016/j.msea.2016.08.048

Warren, J. A. (2015). Workshop summary: Materials genome initiative: Materials data. https://doi.org/10.6028/nist.ir.8038

Wille, T. H., & Schwink, C. H. (1986). Precision measurements of critical resolved shear stress in Cumn Alloys. *Acta Metallurgica*, *34*(6), 1059–1069. https://doi.org/10.1016/0001-6160(86)90216-6

Wilson, P., Field, R., & Kaufman, M. (2016). The use of diffusion multiples to examine the compositional dependence of phase stability and hardness of the Co-Cr-Fe-Mn-Ni high entropy alloy system. *Intermetallics*, *75*, 15–24. https://doi.org/10.1016/j.intermet.2016.04.007

Wu, D., Wang, F., Cheng, J., & Li, C. (2018). Effect of nb and V on austenite grain growth behavior of the CR-mo-V steel for brake discs. *High Temperature Materials and Processes*, *37*(9-10), 899–907. https://doi.org/10.1515/htmp-2017-0077

Wu, X., Liu, R., Zhang, X., & Yao, M. X. (2021). Microstructure and performance characterization of a novel cobalt high-entropy alloy. *Metallurgical and Materials Transactions A, 52*(9), 4066–4089. https://doi.org/10.1007/s11661-021-06365-8

Wu, Z., Bei, H., Pharr, G. M., & George, E. P. (2014). Temperature dependence of the mechanical properties of equiatomic solid solution alloys with face-centered cubic

crystal structures. *Acta Materialia*, *81*, 428–441. https://doi.org/10.1016/j.actamat.2014.08.026

Wu, Z., Gao, Y. F., & Bei, H. (2015). Single Crystal Plastic Behavior of a single-phase, face-center-cubic-structured, equiatomic Fenicrco Alloy. *Scripta Materialia*, *109*, 108–112. https://doi.org/10.1016/j.scriptamat.2015.07.031

Yang, M., Yan, D., Yuan, F., Jiang, P., Ma, E., & Wu, X. (2021). Dynamically reinforced heterogeneous grain structure prolongs ductility in a medium-entropy alloy with Gigapascal yield strength. *Heterostructured Materials*, 585–604. https://doi.org/10.1201/9781003153078-36

Ye, Y. F., Wang, Q., Lu, J., Liu, C. T., & Yang, Y. (2016). High-entropy alloy: Challenges and prospects. *Materials Today*, *19*(6), 349–362. https://doi.org/10.1016/j.mattod.2015.11.026

Youssef, K. M., Zaddach, A. J., Niu, C., Irving, D. L., & Koch, C. C. (2014). A novel low-density, high-hardness, high-entropy alloy with close-packed single-phase nanocrystalline structures. *Materials Research Letters*, *3*(2), 95–99. https://doi.org/10.1080/21663831.2014.985855

Zaddach, A. J., Scattergood, R. O., & Koch, C. C. (2015). Tensile properties of low-stacking fault energy high-entropy alloys. *Materials Science and Engineering: A*, *636*, 373–378. https://doi.org/10.1016/j.msea.2015.03.109

Zhang, C., Chen, G. J., & Dai, P. Q. (2016). Evolution of the microstructure and properties of laser-clad fecrnicobx high-entropy alloy coatings. *Materials Science and Technology*, *32*(16), 1666–1672. https://doi.org/10.1080/02670836.2015.1138035

Zhang, Y., Ma, W.-G., Zhang, R.-Y., Chen, C., & Guo, L. (2014). QCD NLO and EW NLO corrections Tott¯Hproduction with top quark decays at hadron collider. *Physics Letters B*, *738*, 1–5. https://doi.org/10.1016/j.physletb.2014.09.022

Zhang, Y., Zhou, Y. J., Lin, J. P., Chen, G. L., & Liaw, P. K. (2008). Solid-solution phase formation rules for multi-component alloys. *Advanced Engineering Materials*, *10*(6), 534–538. https://doi.org/10.1002/adem.200700240

Zhang, Z., Sheng, H., Wang, Z., Gludovatz, B., Zhang, Z., George, E. P., Yu, Q., Mao, S. X., & Ritchie, R. O. (2017). Dislocation mechanisms and 3D twin architectures generate exceptional strength-ductility-toughness combination in CrCoNi medium-entropy alloy. *Nature Communications*, *8*(1). https://doi.org/10.1038/ncomms14390

ZHAO, J. (2006). Combinatorial approaches as effective tools in the study of phase diagrams and composition–structure–property relationships. *Progress in Materials Science*, *51*(5), 557–631. https://doi.org/10.1016/j.pmatsci.2005.10.001

Zhao, J.-C., Peluso, L. A., Brewer, L. N., & Jackson, M. R. (2003). Diffusion multiples for high-efficiency alloy design. *High-Throughput Analysis*, 349–375. https://doi.org/10.1007/978-1-4419-8989-5_16

Zhao, Y. L., Yang, T., Tong, Y., Wang, J., Luan, J. H., Jiao, Z. B., Chen, D., Yang, Y., Hu, A., Liu, C. T., & Kai, J.-J. (2017). Heterogeneous precipitation behavior and stacking-fault-mediated deformation in a cocrni-based medium-entropy alloy. *Acta Materialia*, *138*, 72–82. https://doi.org/10.1016/j.actamat.2017.07.029

Zhong, X., Zhang, Q., Jiang, F., Yan, Y., Wang, Z., & Wu, M. (2021). Microstructural features and excellent compression properties of a novel al0.7cocrfeniti0.3 high entropy alloy. *Materials Letters*, *286*, 129246. https://doi.org/10.1016/j.matlet.2020.129246

Zhou, R., Liu, Y., Zhou, C., Li, S., Wu, W., Song, M., Liu, B., Liang, X., & Liaw, P. K. (2018). Microstructures and mechanical properties of C-containing fecocrni high-entropy alloy fabricated by selective laser melting. *Intermetallics*, *94*, 165–171. https://doi.org/10.1016/j.intermet.2018.01.002

Zhu, Z. G., Ma, K. H., Yang, X., & Shek, C. H. (2017). Annealing effect on the phase stability and mechanical properties of (fenicrmn)(100−)co high entropy alloys. *Journal of Alloys and Compounds*, *695*, 2945–2950. https://doi.org/10.1016/j.jallcom.2016.11.376